JOURNAL OF GEOPHYSICAL RESEARCH, VOL. 113, D08213, doi:10.1029/2006JD007709, 2008

Kinematic, microphysical, and electrical aspects of an asymmetric bow-echo mesoscale convective system observed during STEPS 2000

Timothy J. Lang[1] and Steven A. Rutledge[1]

Received 28 June 2006; revised 25 October 2007; accepted 28 December 2007; published 30 April 2008.

[1] Five hours of detailed observations of the asymmetric bow-echo mesoscale convective system on 11–12 June 2000 during the STEPS project are presented. Data sources included polarimetric and Doppler radars, a VHF lightning mapper, and the National Lightning Detection Network. Nearly every (99%) VHF lightning source occurred within 10 km of the convective line. Charge identification within the much of the convective line revealed evolution during the first 3 h from a normal polarity dipole (upper positive charge near 9 km MSL/−30°C, over mid-level negative charge near 7 km/−16°C) to a normal polarity tripole with the addition of lower positive charge near 4 km (1°C). During the final 2 h, the charge structure resembled an inverted dipole, with negative charge overlaying positive. When the bow echo occurred during hour 2, part of the cells associated with severe winds developed an inverted tripolar charge structure and produced predominantly positive cloud-to-ground lightning. Stratiform lightning was infrequent, normally initiating in the convective line and propagating rearward along two pathways: a downward-sloping upper pathway near 9 km, and a more common constant-altitude lower pathway near 6 km (−10°C). Some flashes initiated within the stratiform region during this time, but only after stratiform reflectivities increased significantly in the mixed-phase region. These flashes initiated near the bright band (4 km), and tapped negative charge above and positive charge below. Possible mechanisms to explain the observations are discussed.

Citation: Lang, T. J., and S. A. Rutledge (2008), Kinematic, microphysical, and electrical aspects of an asymmetric bow-echo mesoscale convective system observed during STEPS 2000, *J. Geophys. Res.*, *113*, D08213, doi:10.1029/2006JD007709.

1. Introduction

[2] Despite considerable research concerning electrification and lightning production in mesoscale convective systems (MCSs), many unanswered questions remain. This study addresses three questions described in the following subsections, using an observational case study of the evolution of an asymmetric bow-echo MCS.

1.1. What is the Distribution of Total Lightning and Charge in Asymmetric and Bow-Echo MCSS, and How Well Does This Agree With Conceptual Models?

[3] The vast majority of past MCS electrification studies have focused on either cloud-to-ground (CG) lightning [e.g., *Rutledge and MacGorman*, 1988] or electrical charge structure as revealed by balloon-borne electric field meter soundings [e.g., *Stolzenburg et al.*, 1998]. *Stolzenburg et al.* [1998] presented a conceptual model of charge structure in a archetypal MCS. Their findings suggested that, within the updrafts of the convective line of MCSs, there are four layers of alternating charge, with two additional layers outside updrafts. Within the transition zone behind the convective line there are usually five charge layers, while in the stratiform precipitation region there are usually up to six. *Stolzenburg et al.* [1998] suggested that upper charge layers in the convective line are connected to their counterparts in the stratiform region, and may slope downward toward the rear of the MCS, a hypothesis supported by observations from *Stolzenburg et al.* [2001] and *Carey et al.* [2005].

[4] *Marshall and Rust* [1993] concluded that, despite this conceptual model, there can be significant variability in stratiform charge structure. They identified two archetypal charge structures, Type A and Type B. Type A has five charge layers, with negative charge near 0°C, and is representative of the stratiform regions of squall lines and predominantly stratiform MCSs (see *Houze et al.* [1990] for a review of MCS organizational archetypes). They found a simpler charge structure, Type B, in bow-echo MCSs. Type B has four alternating charge layers with positive charge near 0°C. *Schuur and Rutledge* [2000a], in their observations, found charge layers in symmetric MCSs to most closely follow the Type A paradigm. However, asymmetric MCSs had simpler structures more akin to Type B.

[5] Recently, *Carey et al.* [2005] studied total lightning in a symmetric leading-line, trailing- stratiform MCS using a three-dimensional (3D) VHF lightning mapper. Within the convective line, which contained most of the observed lightning, the lightning distribution suggested a normal-

[1]Department of Atmospheric Science, Colorado State University, Fort Collins, Colorado, USA.

0148-0227/08/2006JD007709$09.00

polarity tripolar electrical structure, with positive charge near 3°C and −35°C, and negative charge near −17°C. Another notable result was a downward-sloping lightning pathway from the upper positive charge region, which terminated 40–50 km into the stratiform region near the altitude of the radar bright band. A possible origin of this sloping pathway, as discussed by *Carey et al.* [2005], was positive charge residing on snow particles ejected rearward from the convective line, which gradually descend toward the melting level.

[6] *Carey et al.* [2005] found evidence for stratiform lightning of all types to occur within three positive charge layers in the stratiform region, at 2°C, −11°C, and −31°C. *Lyons et al.* [2003], in a study of MCS sprite-producing stratiform positive CG (+CG) flashes, found corresponding VHF source densities in these flashes to concentrate near the melting level, implying positive charge near 0°C. *Lang et al.* [2004a], in a study of MCS +CGs terminating in the stratiform region, found corresponding VHF source densities to concentrate near −10°C. Thus these latter two studies combined found individual stratiform positive charge layers that correspond to two of the three layers found by *Carey et al.* [2005].

[7] Still missing from the literature is a comprehensive study of the total lightning distribution in asymmetric MCSs. A reasonable hypothesis with such systems is that their lightning distribution and charge structure also could be asymmetric, with significant variability along the convective line not seen in symmetric storms as by *Carey et al.* [2005]. In addition, their stratiform lightning distribution could be more representative of the simpler Type B archetype, with positive charge near 0°C and perhaps again near −20°C [*Marshall and Rust*, 1993; *Schuur and Rutledge*, 2000a].

1.2. What Physical Mechanisms Account for the Observed Bipolarity in MCS CG Lightning Distribution, as Well as the Initiation of Lightning Within the Stratiform Region of MCSs?

[8] The typical CG lightning pattern in mature MCSs is bipolar, with negative CG (−CG) lightning striking predominantly within the convective line, while +CG lightning dominates in the stratiform region [e.g., *Hill*, 1988; *Orville et al.*, 1988; *Rutledge and MacGorman*, 1988; *Stolzenburg*, 1990; *Rutledge et al.*, 1990]. Recent studies of MCS lightning using VHF mappers have noted that the vast majority of flashes propagating within the stratiform region initiated within the convective line, and traversed through the stratiform region along well-defined pathways that likely corresponded to the locations of significant charge layers [e.g., *Lang et al.*, 2004a, *Carey et al.*, 2005]. However, *Lang et al.* [2004a] also noted a minority of stratiform +CG flashes that actually initiated within the stratiform region itself.

[9] There remains considerable uncertainty as to what mechanism could explain sufficient electric fields to initiate lightning within the stratiform region. The two candidates are charge advection and in situ charging [*Rutledge and MacGorman*, 1988]. There have been numerous studies of these processes. *Rutledge et al.* [1993] and *Rutledge and Petersen* [1994] suggested in situ charging as the dominant mechanism, with the latter study finding that stratiform lightning (in particular, +CGs) only occurs when vertical reflectivity profiles are intense (>15 dBZ above the melting level). This suggests that a non-inductive charging mechanism may be important for charge separation in the stratiform region. Other explanations for charging mechanisms include inductive mechanisms or charging during melting [*Shepherd et al.*, 1996].

[10] However, *Carey et al.* [2005] presented evidence for lightning occurring along rearward advected ice particle pathways, implying that advection of charge from the convective line could be important in the upper levels of the stratiform region. In the modeling study of *Schuur and Rutledge* [2000b], in situ charge separation explained up to 70% of the total charge in the stratiform region, with charge advection accounting for 30%. *Rutledge et al.* [1990] suggested that both stratiform region charging mechanisms might account for different subsets of stratiform +CGs. Thus it is possible that both mechanisms may be important in stratiform charging, and together could account for both the initiation and the propagation of stratiform lightning. However, in order to test this idea, further observations of MCS lightning are required, including 3D mapping of channels. As part of this, it is important to understand where lightning initiates within the stratiform region.

1.3. Are There Lightning Patterns Characteristic of Bow-Echo MCSs, Which May be Useful in the Context of Understanding and Predicting Severe Weather, and if so What Causes Them?

[11] One of the most robust relationships between lightning and severe weather is the common occurrence of a rapid increase in total (intracloud or IC, and CG) lightning flash rate several minutes prior to the onset of severe weather, such as large hail (diameter D > 2 cm) or tornadoes [*Williams et al.*, 1999]. *Williams et al.* [1999] interpreted this as a consequence of rapid intensification of the convective updraft, leading to increases in both total lightning flash rate and the probability of severe weather. Thus it may be possible to associate total flash rate in the convective line of MCSs with bow echoes and severe winds, as well as large hail production.

[12] There also may be a relationship between severe weather and CG lightning in MCSs. *Price and Murphy* [2002] noted an enhancement of +CG fraction during damaging wind events associated with a bow-echo MCS [e.g., *Weisman*, 2001]. During the derecho phase, +CG fraction exceeded 70% for over 3 h. *Price and Murphy* [2002] did not discuss the location of these +CGs relative to the convective line or stratiform region. However, *Nielsen et al.* [1994] and *Knupp et al.* [1998] both noted that +CGs could be enhanced in the convective line of a MCS during its development phase, when rapid intensification of the convection was occurring.

[13] Given the commonly observed correspondence between storms that produce predominantly +CG lightning and severe weather such as hail, strong winds, and tornadoes [e.g., *Rust et al.*, 1981a, 1981b; *Stolzenburg*, 1994; *Carey and Rutledge*, 1998], it is reasonable to hypothesize that portions of the convective line involved with the strongest winds (as well as large hail) also may feature enhanced +CG lightning. This could be particularly true in the U.S. Central Plains [*Carey et al.*, 2003].

The underlying mechanism may be the creation of an inverted charge structure akin to the +CG-dominated storm studied by *Wiens et al.* [2005], with significant positive charge at mid-levels (−10 to −20°C). This may occur via the acquisition of positive charge on riming particles (graupel or hail) during rebounding collisions with ice crystals. *Saunders and Peck* [1998] found that high riming accretion rates lead to positive charging of the riming particle, even at cold temperatures. The riming accretion rate could be boosted by enhanced liquid water contents that may exist within strong, broad updrafts [e.g., *Williams et al.*, 2005]. The modeling study of *Kuhlman et al.* [2006] supported this theory by showing that charging parameterizations based on *Saunders and Peck* [1998] could lead to the development of inverted charge structures.

2. Brief Overview of Case Study

[14] During the afternoon of 11 June 2000 (local time), an asymmetric bow-echo MCS developed and propagated through the domain of the Severe Thunderstorm Electrification and Precipitation Study (STEPS) [*Lang et al.*, 2004b]. This is the same storm whose stratiform +CG lightning was studied by *Lang et al.* [2004a].

[15] The synoptic setting for this MCS featured mostly zonal flow at upper levels over Colorado and Kansas, with the axis of the jet stream much further to the north. Southeasterly flow existed at the surface, with dewpoints in the 7–9°C range. A sounding launched at 1813 UTC (hereafter all times in UTC) approximately 100 km west of Goodland, KS, showed 936 J kg^{-1} of convective available potential energy. The mean shear from the surface to 6 km AGL and bulk Richardson number calculated via the method of *Weisman and Klemp* [1986] were 9.0 m s^{-1} and 23.1, respectively. Though consistent with the development of intense multicellular convection and squall lines [e.g., *Weisman and Klemp*, 1986], the environmental thermodynamics and shear did not suggest the likelihood of bow echoes [*Weisman*, 1993].

[16] The MCS started out by 1900 as a collection of cells that appeared over the Colorado counties of Elbert and El Paso, southeast of Denver. By 2030 the storm had a well-defined southwest-northeast-oriented linear structure, with trailing stratiform echo forming by 2130. Individual cell lifetimes normally were 0.5–1 h, and no supercells were observed in the MCS. The MCS was well-covered by the STEPS radar and lightning observing network for nearly 5 h (2100 on 11 June through 0150 on 12 June), during which time it produced numerous reports of severe weather, including large hail and strong winds. This MCS also underwent dramatic kinematic, microphysical, and electrical evolution, which was examined in detail.

3. Data and Methodology

3.1. Radars

3.1.1. Overview

[17] *Lang et al.* [2004b] provided a detailed overview of the STEPS experimental design, so only the portions most pertinent to this study will be covered here. Polarimetric and Doppler radar data were available from both the NCAR S-Pol and CSU-CHILL radars. Since the CHILL scan strategy was not optimal, only data from S-Pol (but not from CHILL) were used in the analyses to be presented. A third Doppler radar, the WSR-88D NEXRAD at Goodland, KS (KGLD), was available for this study. The KGLD radar was ideal for full time series analysis of the storm, since it scanned the entire MCS every 5–6 min throughout the observation period.

3.1.2. Polarimetric Analysis

[18] Due to the size of the MCS and scanning restraints with polarimetric radars, it was impossible to construct well-resolved time series of the entire MCS with polarimetric data. Hence analyses of select portions of the MCS were done. Otherwise, data quality control and analysis methodology were virtually identical to *Tessendorf et al.* [2005]. In particular, polarimetric data were interpolated to 0.5 × 0.5 × 0.5 km^3 resolution Cartesian grids (spanning 75 km in either horizontal direction, and 1.5–20 km MSL in the vertical) covering regions of interest, and the *Tessendorf et al.* [2005] fuzzy-logic hydrometeor identification (HID) methodology was used to construct time series and cross-sections of variables such as graupel echo volume. One difference with the *Tessendorf et al.* [2005] methodology was that the REORDER software was used for creating grids.

3.1.3. Dual-Doppler Analysis

[19] High-resolution grids similar to the polarimetric ones were created for select portions of the storm, using reflectivity and radial velocity data from S-Pol and KGLD. These grids were used in dual-Doppler syntheses to obtain 3D kinematic information. The synthesis procedure was very similar to the methodology of *Tessendorf et al.* [2005], except radial velocity was manually unfolded instead of using an automated algorithm. In all dual-Doppler figures in this paper the winds shown are relative to ground.

3.1.4. Convective/Stratiform Partitioning

[20] In addition to the high-resolution grids, every KGLD volume within the analysis period was interpolated to a 2 × 2 × 0.5 km^3 resolution grid (spanning 376 km in either horizontal direction, and 1.5–20 km MSL in the vertical) centered 28 km north and 62 km west of the KGLD radar. Using these coarser grids, the convective and stratiform portions of this storm were separated objectively, in order to examine the evolution of radar reflectivity and lightning in these different areas. However, it was found that conventional partitioning algorithms [*Steiner et al.*, 1995; *Yuter and Houze*, 1998] failed on the intense stratiform region of this MCS, in which major areas were misclassified as convective even after extensive tuning of the algorithms. Therefore a new partitioning algorithm was developed utilizing information in the vertical. When 30+ dBZ was observed at 6+ km MSL (−10°C; hereafter all altitudes in MSL), the associated grid column was classified as convective. If this was not the case but the grid column was within 10 km distance of a convective grid column, the column was classified as transition. If neither condition was satisfied, the grid column was stratiform. Grid columns containing missing data at 6+ km, such as those within the KGLD cone of silence, were unclassified.

[21] The subjectively chosen height and reflectivity thresholds were lightning-based, and corresponded loosely to the rule of thumb developed by *Petersen et al.* [1996] that most storms do not become electrified until they show 30+ dBZ echo at −10°C. Since this was a lightning study,

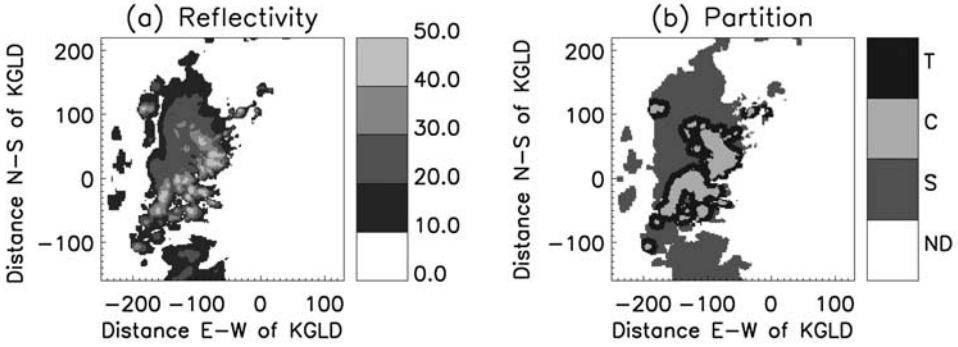

Figure 1. Horizontal cross-section of KGLD reflectivity at 6 km MSL, at 2200 UTC on 11 June (a), and the results of the convective/stratiform partitioning algorithm (b); C, Convective; S, Stratiform; T, Transition; ND, No Data).

it was felt that such an algorithm was justified. No major microphysical or dynamical inferences were made on the basis of this algorithm. For example, convective grid columns included only the most intense convection, which in turn was likely to produce lightning. The transition columns should not be confused with the transition zone of MCSs [*Houze et al.*, 1990], although they certainly could include such portions of the storm. The transition columns likely contained weak and decaying convection in the vicinity of the convective line, while stratiform columns contained both stratiform echo and perhaps weak/decaying convection far (>10 km) from major convection.

[22] Figure 1 shows an example of the performance of this algorithm for one particular KGLD volume. It effectively picked out the convective line from the surrounding echo, and avoided the misclassification of the intense stratiform echo as convective. In addition, though no major dynamical inferences should be based on this algorithm, an intercomparison was performed between 12 partitioned KGLD volumes matched in time with 12 dual-Doppler synthesis volumes degraded to 2-km horizontal resolution. Maximum vertical velocity was determined in each grid column, separated by partition category. The median results were 4.0 m s^{-1} in convective columns, 1.3 m s^{-1} in tran-

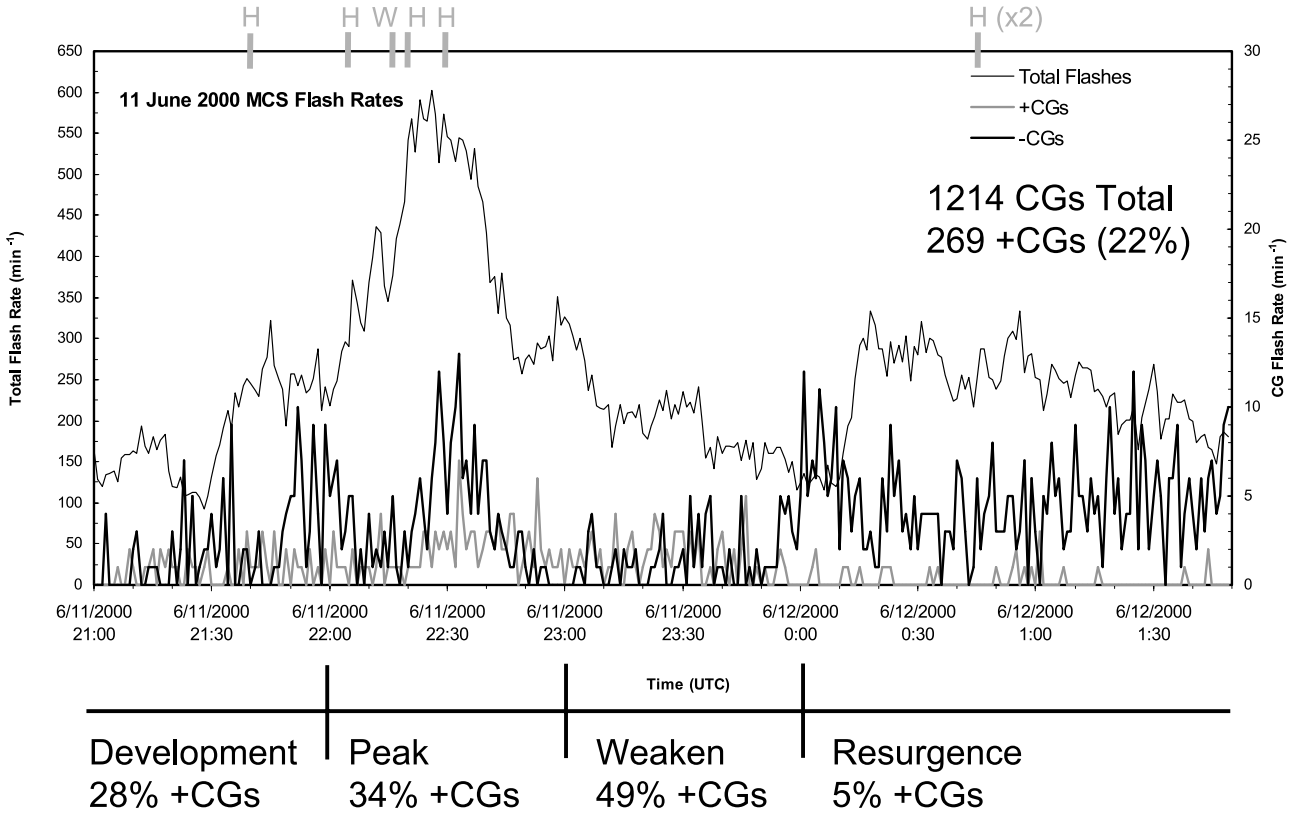

Figure 2. Time series of 1-min total flash rate (required LMA stations $\geq$ 6, and $\chi^2 \leq 2.0$ for VHF source locations) and CG flash rates. Also shown are the times of severe weather (W, Wind; H, Hail) and statistics on +CG percentage.

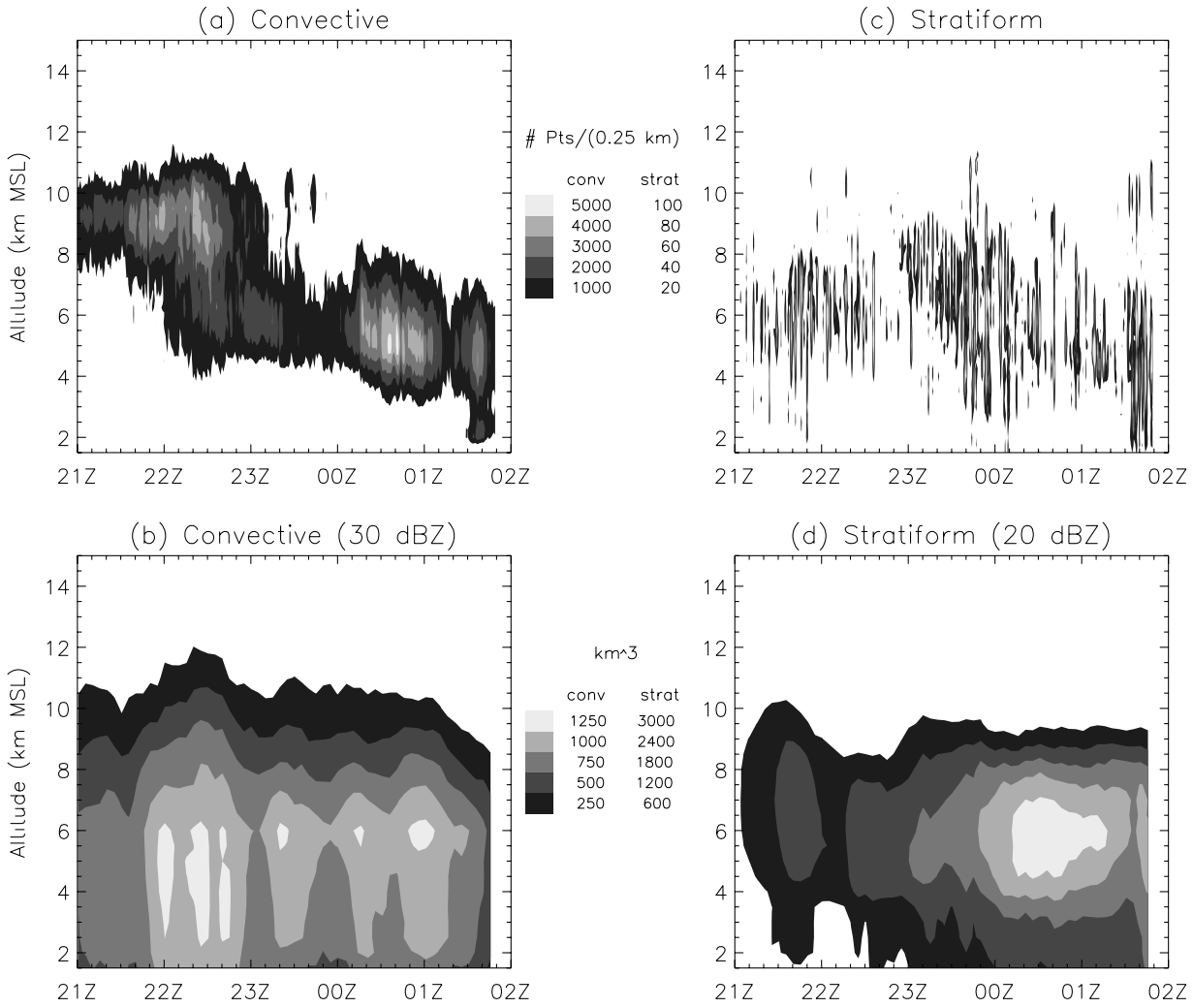

Figure 3. Time-height plots of VHF source density in the convective (a) and stratiform (c) regions of this MCS. Also shown are time-height plots of 30 dBZ echo volume in the convective region (b), along with 20 dBZ echo volume in the stratiform region (d).

sition columns, and 0.9 m s^{-1} in stratiform columns, in line with expectations for vertical velocity trends in these different categories. Therefore the algorithm should be adequate for developing gross statistics on lightning and reflectivity evolution within the convective and stratiform regions of this MCS.

3.2. Three-Dimensional VHF Lightning Mapping Array

3.2.1. Overview

[23] The New Mexico Tech Lightning Mapping Array (LMA) provided 3D mapping of lightning channels at high spatial and temporal resolution [*Rison et al.*, 1999]. Within the 70-km diameter core of the 13-station STEPS LMA network, centered within the triangle formed by the three radars [*Lang et al.*, 2004b], *Thomas et al.* [2004] claimed an uncertainty in source locations of 6–12 m in the horizontal and 20–30 m in the vertical. Outside the network core, range and altitude errors increased as ranged squared, while azimuthal errors increased linearly with range [*Thomas et al.*, 2004]. Vertical resolution was <1 km out to 125 km from the network center, which encompassed all of the radar dual-Doppler lobes [*Lang et al.*, 2004b]. Normally, only VHF sources detected by at least 7 stations were examined, and goodness-of-fit values (χ^2) were required to be ≤ 1.0 in the source location solutions. Exceptions will be noted in figure captions.

[24] Since this MCS spanned up to ~200 km along its convective line, and was observed for almost 5 h, there were times when the LMA resolved lightning better than others, particularly in the vertical. Lightning was most poorly resolved during the 2100 hour and the 0100 hour. Observations in the convective line were best during the 2200 hour, while stratiform region observations were best during the 2300 hour. In the discussion of results, the distance of the relevant portions of the storm from the LMA network center will be noted.

3.2.2. Flash Rates and Flash Classification

[25] Flashes were identified and categorized, and flash rate calculations were made, using the lightning viewing software called XLMA, following the methodology of *Thomas et al.* [2003]. No changes were made to the software defaults for flash sorting. This algorithm is automated, and is subject to errors such as grouping the wrong

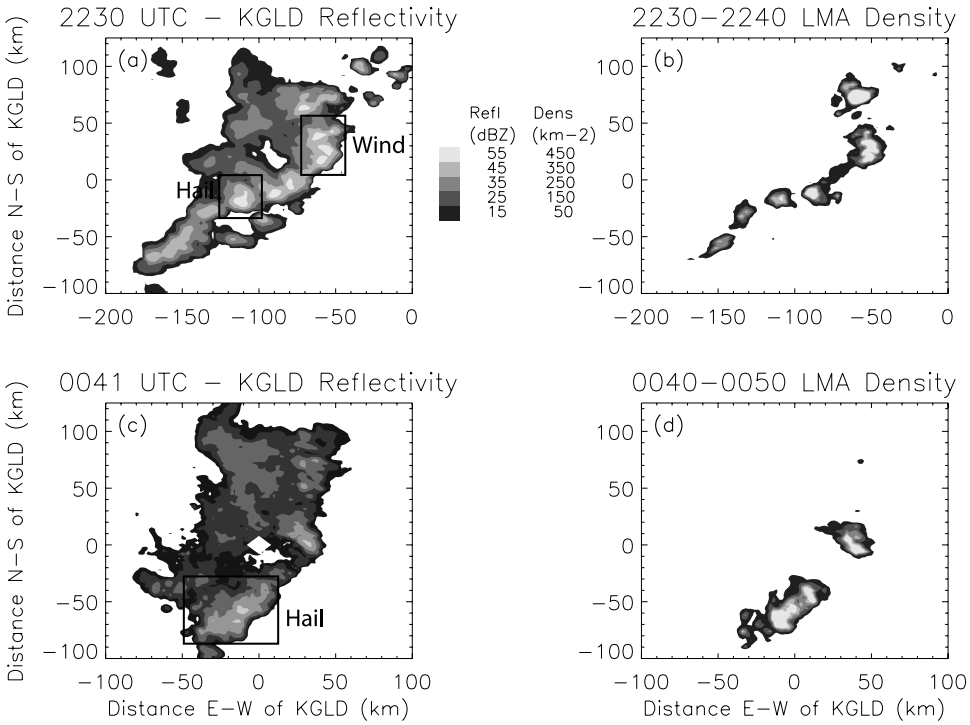

Figure 4. (a) Horizontal cross-section at 1.5 km MSL of KGLD reflectivity at 2230 UTC for the entire MCS. Also highlighted are the early hail and severe wind cells examined in this study. (b) Plan projection of VHF source density during 2230–2240 UTC, for the same domain as Figure 4a. (c) Same as Figure 4a but for the MCS at 0041 UTC. Also highlighted are the late hail cells examined in this study. (d) Same as Figure 4b but for 0040–0050 UTC.

sources with the wrong flashes. However, as *Wiens et al.* [2005] noted, sensitivity studies suggest that basic flash trends are preserved.

[26] VHF sources were classified as convective, transition, or stratiform if they occurred in the respective grid column of the temporally closest KGLD volume. A flash was determined to be convective if 80% or more of the sources occurred in convection. Similarly, stratiform flashes were those with $\geq$ 80% sources in stratiform. Other flashes were classified as mixed. Median location of the first 10 sources or first 10% of total sources in a flash (whichever was less) was determined and named the origin location of that flash, which was similarly classified as convective, transition, or stratiform.

3.2.3. Charge Identification

[27] Manual charge identification using the LMA data was performed following the technique and theory of *Rison et al.* [1999], *Thomas et al.* [2001], *Rust et al.* [2005], and *Wiens et al.* [2005]. This technique assumes the bidirectional electric field breakdown model for lightning discharges proposed by *Kasemir* [1960] and further advocated by *Mazur and Ruhnke* [1993]. It also is based on the fact that negative breakdown through positive charge layers is inherently more noisy at VHF than positive breakdown though negative charge, leading to more VHF sources being detected in positive charge layers than in negative [*Rison et al.*, 1999]. The technique usually assigns charge for a flash within a charge dipole based on the initial vertical direction of the negative leader discharge. If upward, then the dipole is assumed to be positive charge over negative charge; if downward, the opposite. Relative distribution of VHF sources with altitude also can be used to help identify charge locations. This technique is inherently subjective, and is prone to error if its key assumptions are not valid, but its results show good agreement with charge distributions inferred from balloon-borne electric field soundings [*Coleman et al.*, 2003; *Rust et al.*, 2005], and it has been successfully applied by other researchers [e.g., *Wiens et al.*, 2005] to infer physically reasonable gross charge distributions in thunderstorms. Because of the large number of flashes in this MCS, charge was sorted only for selected short time periods (1–10 min each) and locations.

3.3. Other Data

[28] The National Lightning Detection Network (NLDN) data were analyzed following *Wiens et al.* [2005]. Similar to the LMA flash classification, strike locations were classified as convective, transition, or stratiform based on comparisons with KGLD grids. The NLDN is known to occasionally misclassify IC flashes as CGs of either polarity [e.g., *Cummins et al.*, 1998]. No corrections were made for this, but it was noted whenever LMA data suggested that NLDN misclassification had occurred. Misclassifications were uncommon enough that they did not seriously impact any results. Temperatures at various altitudes were provided by a balloon sounding launched through the transition zone of the MCS near 2309. Severe weather reports came from the National Climate Data Center and the Storm Prediction Center, and included latitude and longitude locations, so reports could be matched to the MCS. Severe weather reports are susceptible to substantial inaccuracies in timing and location [e.g., *Williams et al.*, 1999; *Witt et al.*, 1998a,

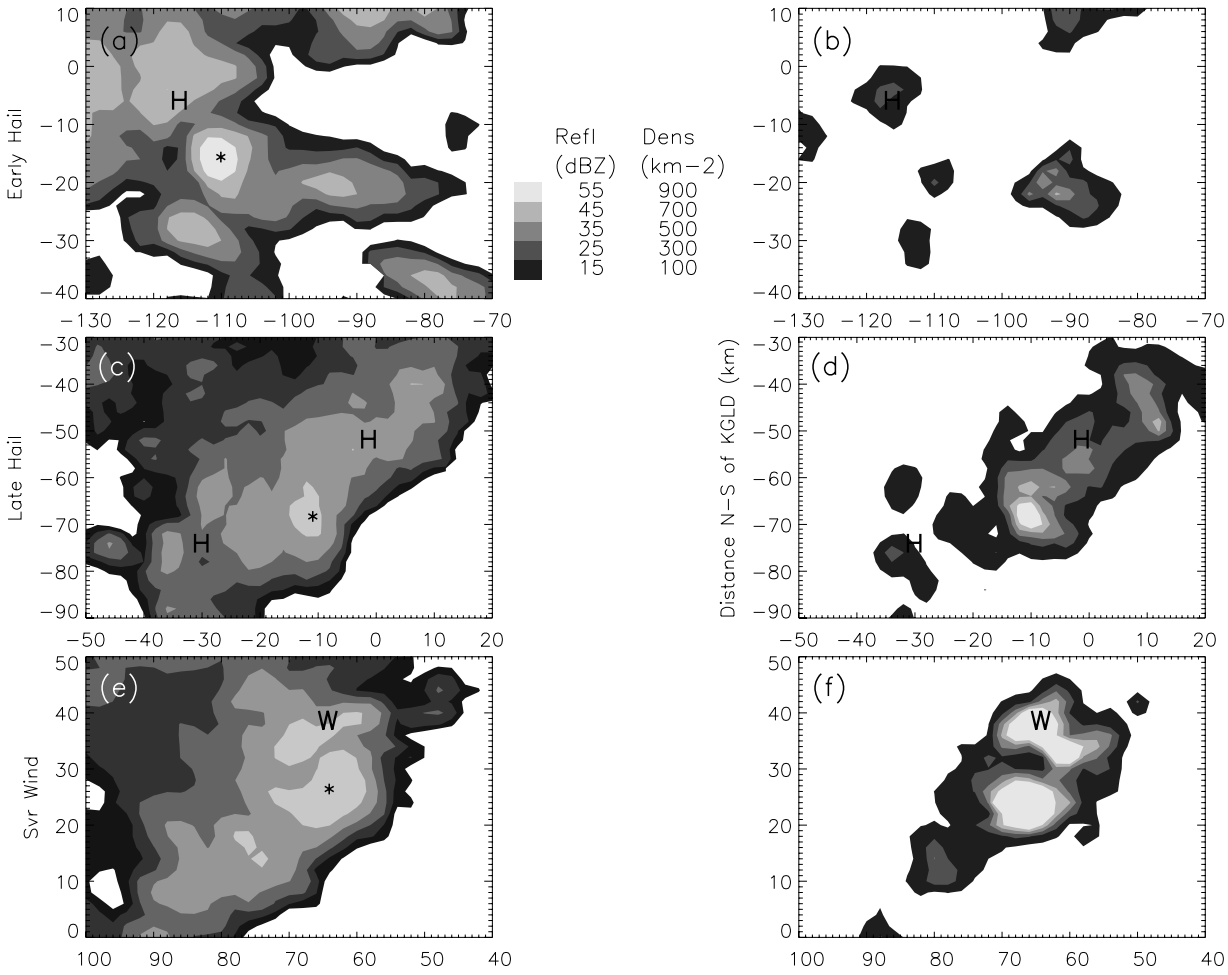

Figure 5. (a) Horizontal cross-section at 1.5 km MSL of KGLD reflectivity at 2205 UTC for the early hail cells. Also highlighted are the location of the severe hail report at 2205 UTC (H), and the northernmost early hail cell (asterisk). (b) Plan projection of VHF source density during 2200–2210 UTC, for the same domain as Figure 5a. The early hail cells were the two southernmost density maxima near −110 km E. (c) Same as Figure 5a but for the late hail cells (center near the asterisk) at 0041 UTC. The reports are for 0045 UTC. (d) Same as Figure 5b but for 0040–0050 UTC. All density maxima were included in the lightning analyses. (e) Same as Figure 5a but for the severe wind cells at 2215 UTC. The 2217 UTC severe wind report location (W) and the approximate region of the strongest near-surface Doppler winds (asterisk) are noted. (f) Same as Figure 5b but for 2210–2220 UTC. All density maxima were included in the lightning analyses.

1998b], so they were interpreted only in the context of corroborating radar data.

4. Observations

4.1. Evolution of the Entire MCS

[29] Figure 2 shows lightning flash rates for the entire MCS during the analysis period (2100–0150). There were two convective peaks in this MCS, both associated with severe weather. One occurred around 2230. During this time period total flash rate peaked near 600 min^{-1}, with −CG flash rates between 10 and 15 min^{-1}, and +CG flash rates between 5 and 10 min^{-1}. Over the 2200 hour roughly one-third of all CGs were positive. Severe weather included up to 3.8-cm diameter hail and wind gusts up to 29 m s^{-1}. This wind report coincided with the bow echo in this storm. The second convective peak occurred after 0000, when CG rates again peaked between 10 and 15 min^{-1}. Total flash rates were still high (∼300 min^{-1}), but lower than the previous peak. Interestingly, during the 0000–0150 time period only 5% of all CGs were positive. During this period there were two reports at 0045 of hail greater than or equal to 2 cm in diameter.

[30] Convection dominated the electrical behavior of this MCS, with total convective VHF sources ∼105 min^{-1} throughout the observation period, while transition regions produced ∼104 sources min^{-1} and stratiform produced ∼103 sources min^{-1}. Thus approximately 99% of all VHF sources occurred in or within 10 km of intense convection. Figure 3 shows time-height distributions of VHF sources and KGLD reflectivity statistics for the portions of the MCS identified as convective and stratiform. Prior to 2200, VHF activity was mainly confined to the upper regions of the convection, around 9 km (−30°C;

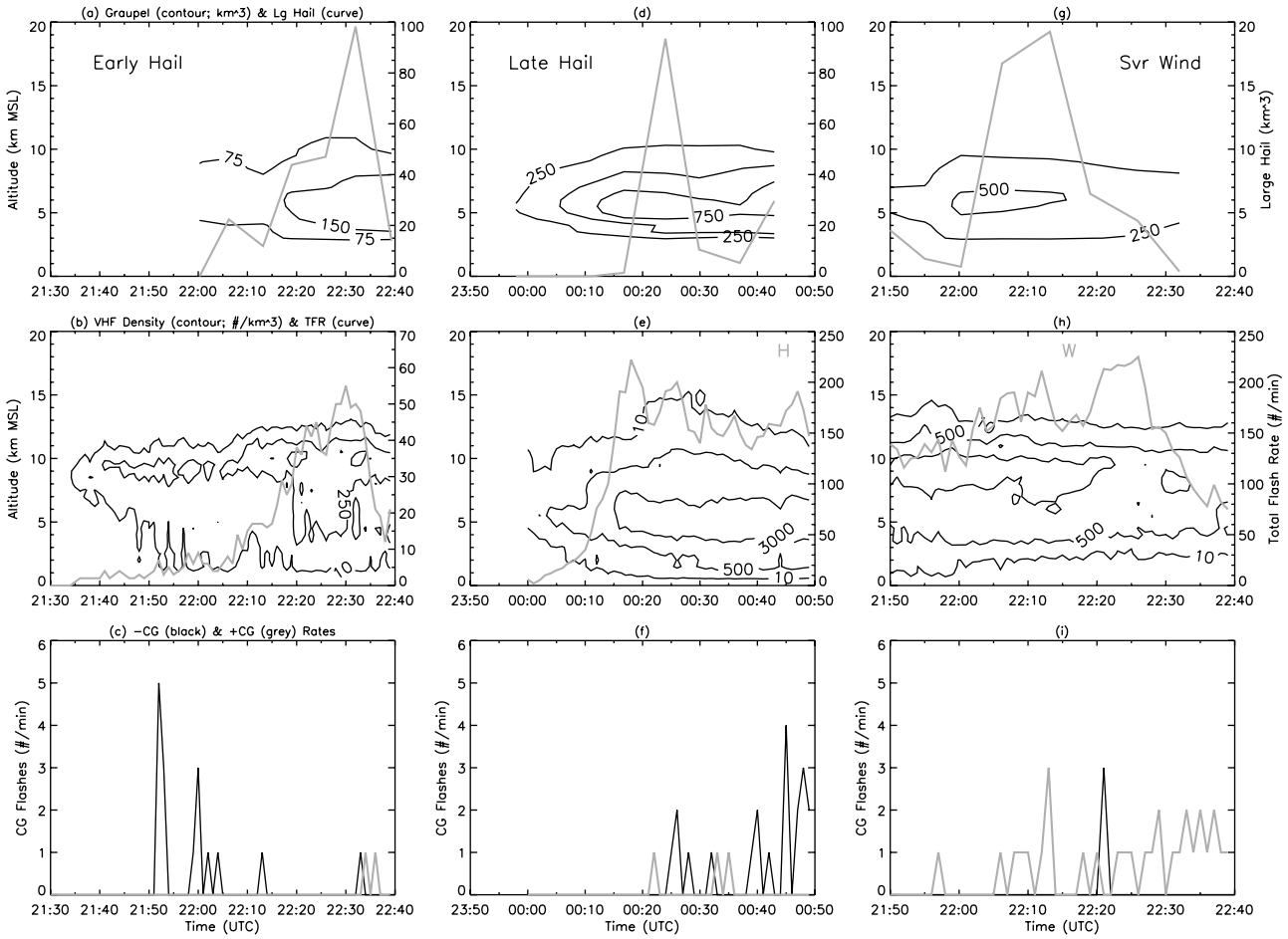

Figure 6. (a) Time-height plot of graupel echo volume (km^3) and time series of large hail echo volume (km^3) for the early hail cells. (b) Time-height plot of VHF source density and time series of total flash rate for the early hail cells. Contours are 10, 250, and 1000 km^{-3}. (c) Time series of CG flash rates for the early hail cells. Also highlighted are times of severe weather. (d) Same as Figure 6a but for the late hail cells. (e) Same as Figure 6b but for the late hail cells, and contours are 10, 500, and 3000 km^{-3}. (f) Same as Figure 6c but for the late hail cells. (g) Same as Figure 6a but for the severe wind cells. (h) Same as Figure 6e but for the severe wind cells. (i) Same as Figure 6c but for the severe wind cells.

Figure 3a). However, after 2200 there was a broadening of the vertical distribution in the convective line, with increasingly more sources at lower altitudes and an eventual decrease in sources aloft. This broadening coincided with increases in total VHF source density and short-lived upward pulses in VHF source altitudes, as well as an increase in total flash rate (Figure 2). After 2300 most LMA activity was centered in the 5–6 km range (−4 to −10°C). This also was true during the second convective peak after 0000, which featured increases in total flash rate (Figure 2), total VHF source density, and short-lived upward pulses in VHF source altitudes.

[31] The downward broadening of convective sources coincided with an increase in convective echo volumes containing 30+ dBZ reflectivity near 5–6 km (Figure 3b). At this altitude (colder than 0°C), the most likely contributors to reflectivities of this magnitude would be graupel and hail. This inference was confirmed using polarimetric radar hydrometeor identification on individual cells, which will be discussed in section 4.2. The convective echo volume contours also increased in altitude roughly corresponding to observed increases in total VHF source density and source altitudes.

[32] Stratiform VHF source densities were small and episodic in nature (Figure 3c). The vertical profile of stratiform reflectivity became relatively intense after 2300, and particularly after 0000 (Figure 3d), with greater than 3000 km3 of 20+ dBZ echo at altitudes between 4.5 and 7 km (all within the mixed-phase region; 0 to −40°C; or 4–10 km). In addition, mean KGLD stratiform reflectivities at 4 km MSL increased steadily from 16 dBZ at 2100 to a peak of 31 dBZ at 0016, and decreased only to 28 dBZ by the end of scanning operations (not shown). Similar trends were seen at other altitudes in the stratiform region.

4.2. Examination of Selected Cells

4.2.1. Overview

[33] Figure 4 shows low-level horizontal cross-sections of KGLD radar reflectivity and plan projections of VHF source density from the LMA at 2230 (a, b) and 0041 (c, d). Also indicated on these plots are cells associated with

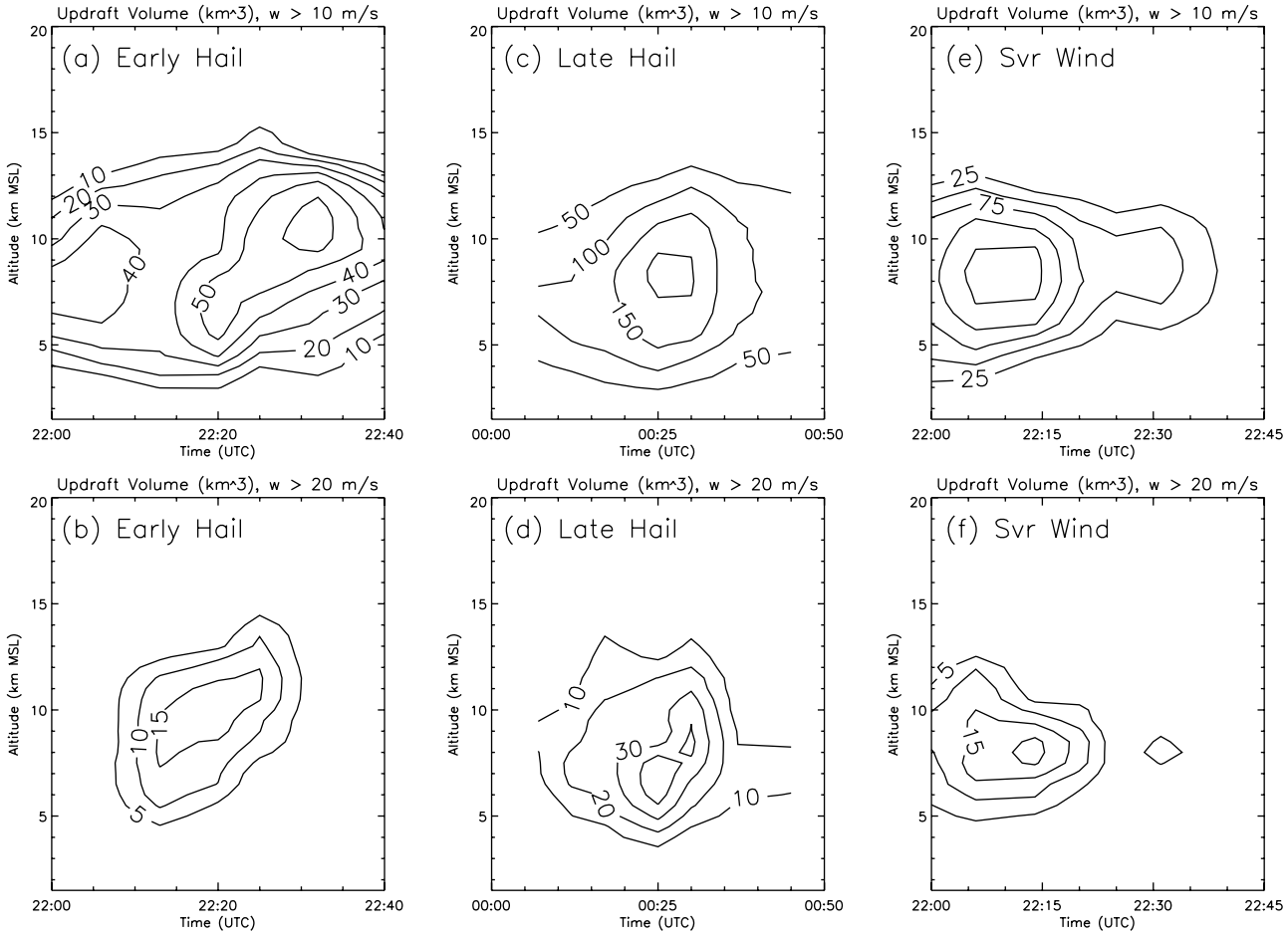

Figure 7. Time-height plots of volume of updrafts greater than 10 m s^{-1} (UV10; (a) and volume of updrafts greater than 20 m s^{-1} (UV20; (b) for the early hail cells. (c) Same as Figure 7a but for the late hail cells. (d) Same as Figure 7b but for the late hail cells. (e) Same as Figure 7a but for the severe wind cells. The largest contour is 125 km^3. (f) Same as Figure 7b but for the severe wind cells.

significant hail and severe wind, which will be discussed in this section. At the earlier time, convection was active all along the leading line of the MCS, and a nascent stratiform region was developing rearward of this line, particularly in the north. There is significant bowing of the convective line, and the cell producing severe winds is contained within this bow echo. (When we refer to "bow echo", we merely mean the portion of the convective line that is bowing, not the entire storm.) By the later time period, the strongest convection was in the southern portion of the MCS, while the mature stratiform region was north of this convection. Overall, the structure of this MCS identifies it as asymmetric [*Houze et al.*, 1990].

[34] The evolution of individual cells associated with significant hail and severe wind was examined. One difficulty with this analysis was that the close proximity of cells made it hard to distinguish them from one another. In addition, there was ambiguity in the assignment of severe weather reports to particular cells. For example, the three severe hail reports between 2200 and 2230 (Figure 2) all occurred within a complex of several closely located cells (within 10–30 km of one another). Considering that up to 75% of severe weather reports are not accurate to within 5 min [*Williams et al.*, 1999], that up to 30% of all severe hail reports cannot be associated with specific radar-observed cells [*Witt et al.*, 1998a, 1998b], and that this storm was located in a rural area where severe weather reporting is limited, we did not always attempt to match hail reports to specific cells. Details of how we treated individual hail reports are given in the following sub-sections.

[35] For the case of severe wind, dual-Doppler syntheses were used to identify the cell with the most intense near-surface winds, which were closest in space and time to the severe wind report. In all cases, VHF source spatial density was plotted against radar data to subjectively isolate (using XLMA) the desired cells from the lightning perspective. Small enough density minima were found between cells in order to effectively isolate them from one another, enough to recover basic trends such as flash rates and vertical evolution of VHF source activity. Figure 5 shows three different sets of cells, examined later in this section, that were responsible for significant hail and severe winds in this MCS.

4.2.2. Early Cells With Significant Hail

[36] The "early hail" cells (Figures 5a and 5b) were a set of two cells that produced significant quantities of radar-inferred large hail (D > 2 cm; i.e., severe-sized). They were a subset of a large complex of cells that was responsible for up to three severe hail reports between 2205 and 2230.

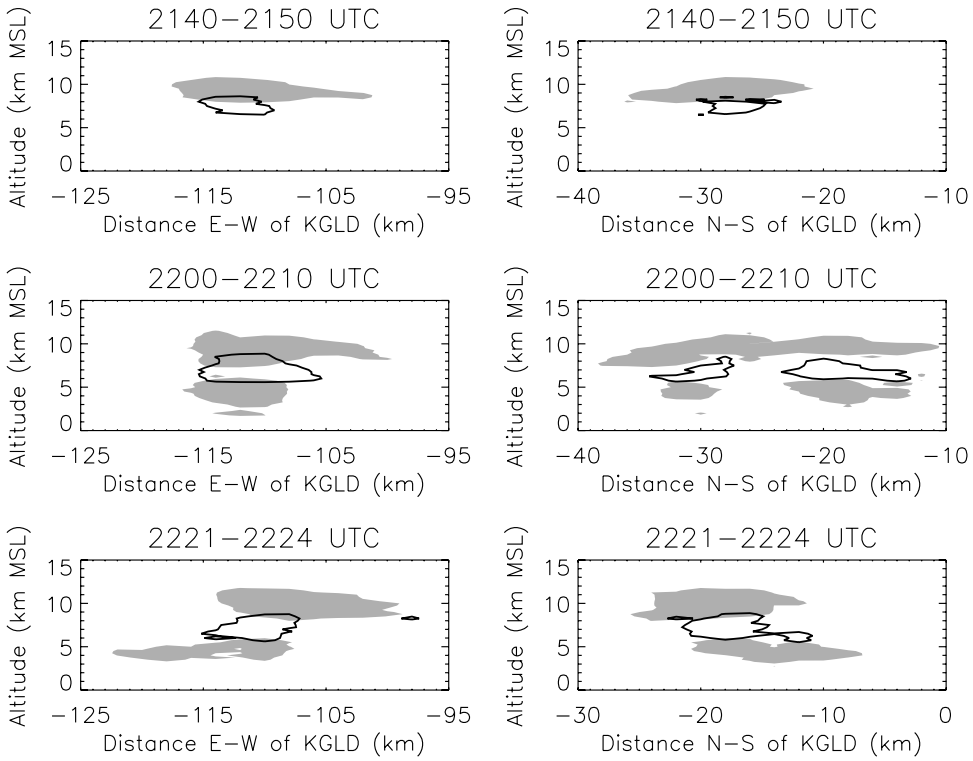

Figure 8. Vertical projections of VHF source density associated with positive (filled gray) and negative (black) charge for three different time periods in the early hail cells, in the E-W (left) and N-S (right) planes. Contour levels are ±60 km^{-2}.

Because of the uncertainties in the reports, we did not match individual cells to severe hail reports. Instead, we chose to examine the two cells we did because they featured interesting microphysical, kinematic, and electrical evolution that was representative of the evolution of much of the convective line around this time. Figures 6a–6c show time series of HID graupel and hail (Figure 6a); VHF source density and total flash rate (b); and CG flash rates (c) for these cells. These cells averaged about 83 km from the LMA network center, within the 1-km vertical resolution threshold for quality 3D analysis.

[37] In general, increasing amounts of polarimetrically identified large hail occurred during a rapid increase in total flash rate, as well as an overall increase in VHF source density and altitudes. There were small spikes in −CG flash rates (Figure 6c) prior to and coincident with the onset of hail, with little +CG activity, but flash rates averaged less than 1 min^{-1}. Thus similar to some of the storms studied by *Lang et al.* [2000] and *Lang and Rutledge* [2002], these cells were associated with few CGs overall.

[38] One of the most interesting results was that downward broadening of VHF source density (from the maximum at 9 km) began when significant graupel was identified at lower altitudes (5–6 km) after 2215 (Figures 6a and 6b). This intensification occurred as the second cell, which originally formed ahead of the convective line, was incorporated fully into the MCS, and could be related to the formation and descent of charge-carrying ice particles from middle to lower levels in the storm [*MacGorman et al.*, 1989].

[39] Figure 7 shows the kinematic evolution of this cell complex, with dual-Doppler updraft volumes greater than 10 m s^{-1} (UV10; Figure 7a) and 20 m s^{-1} (UV20; Figure 7b) plotted as time- height evolution. Both UV10 and UV20 filled most of the mixed-phase region. UV10 reached over 50 km^3 within the mixed-phase region by 2220, as the hail and total lightning time series were rapidly increasing, and the downward broadening in VHF source density was occurring (Figures 6a and 6b). UV20 hit its mixed-phase maximum about 10 min prior to the UV10 maximum.

[40] Figure 8 shows the spatial and temporal evolution of lightning-inferred charge structure in these cells. Early on, the cells contained upper positive charge near 9 km (−30°C), with mid- level negative charge near 7 km (−16°C). Later, the cells developed lower positive charge near 4 km (1°C). In other words, as they intensified the cells evolved from a normal-polarity dipole to a normal tripole [*Williams*, 1989]. Similar evolution was observed in most of the convective line around this time.

[41] Figure 9 shows the microphysical and kinematic structure of these cells at 2213, along with two flashes that revealed the electrical structure. The flashes, an IC between the upper dipole and a −CG involving the mid-level negative and lower positive charge layers, occurred in regions of graupel and hail, near the main updraft of this cell. Note that the lateral displacement of the upper-level dipole to the east late in the complex's lifetime (Figure 8) appeared to be associated with southwesterly flow aloft, as shown in the plotted IC flash (Figure 9).

4.2.3. Late Cells With Severe Hail

[42] Figures 6d–6f show the microphysical and electrical evolution of the cell complex that produced two separate

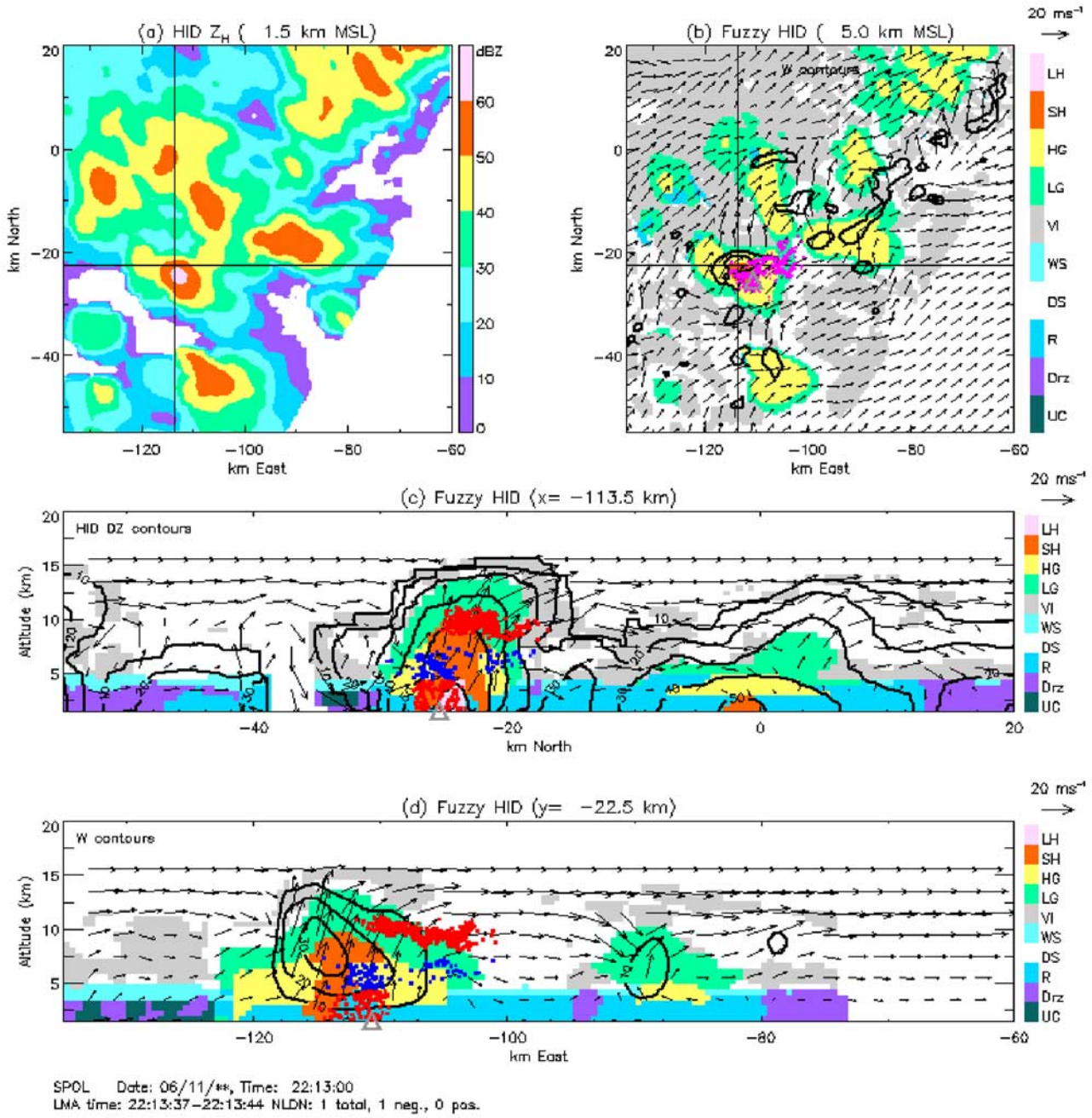

Figure 9. (a) Horizontal cross-section of S-Pol reflectivity for the early hail cells at 2213 UTC. Lines correspond to vertical cross-sections in Figures 9c and 9d. (b) Horizontal cross-section of HID categories (LH, Large Hail; SH, Small Hail; HG, High-Density Graupel; LG, Low-Density Graupel; VI, Vertically Aligned Ice; DS, Dry Snow; WS, Wet Snow; R, Rain; Drz, Drizzle; UC, Unclassified), along with ground-relative dual-Doppler winds, updrafts (contours every 10 m s^{-1}), and VHF sources associated with two flashes at 2213 UTC. A −CG strike location associated with one of the flashes is shown as a gray triangle. (c) Vertical cross-section of HID, reflectivity (line contours), and ground-relative dual-Doppler winds, along with a vertical projection of all VHF sources separated by charge (red, positive; blue, negative). (d) Vertical cross-section of HID, updrafts (line contours), ground-relative dual-Doppler wind vectors, along with a vertical projection of all VHF sources separated by charge (red, positive; blue, negative). Distances relative to KGLD.

reports of 2 and 2.2-cm severe hail at 0045 (Figures 5c and 5d). As this complex contained the only significant convection within 30 km of the hail reports, we feel confident in associating it with the reports. These cells averaged 71 km from the LMA network center. Though there was an increase in hail after 0040, large hail echo volume peaked near 0025 (Figure 6d). However, there was a rapid increase in total flash rate, VHF source density, and

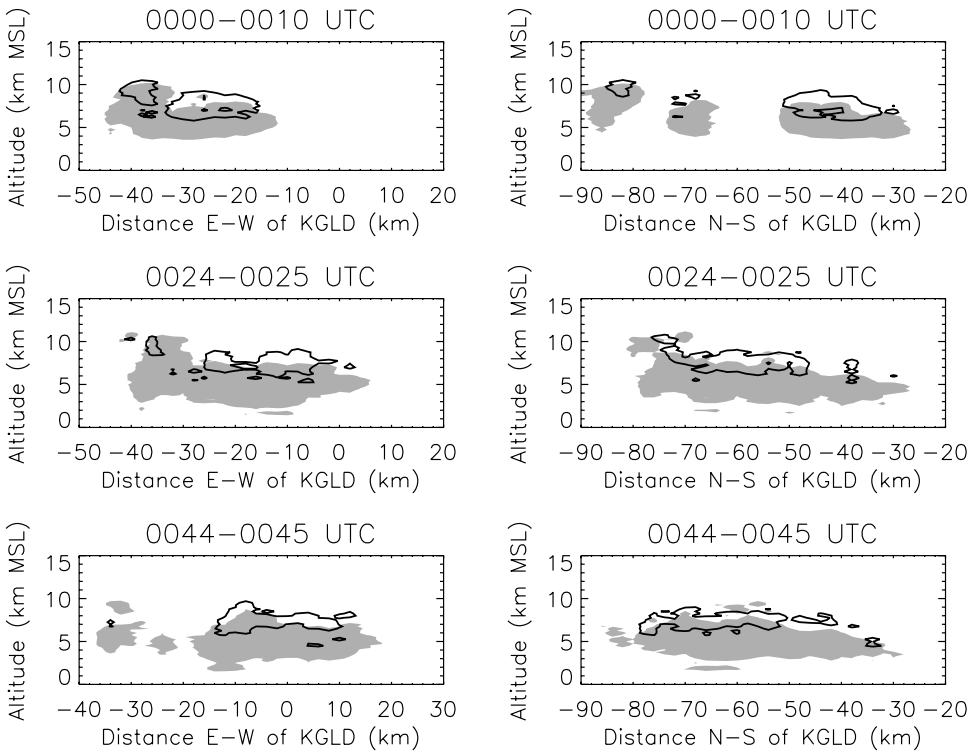

Figure 10. Same as Figure 8 but for the late hail cells, and contour levels are ±30 km^{-2}.

maximum height of VHF sources (~15 km MSL) prior to 0020, providing warning that these cells were intensifying and had severe weather potential (Figure 6e).

[43] Similar to the early hail cells, CG lightning activity was very low (<1 min^{-1}); however, there was an increase in −CG flash rate after 0040 (Figure 6f). Unlike the earlier period (Figure 6b), there was no maximum in VHF source density located near 9 km MSL (Figure 6e). Recall that this cell complex occurred during the second convective peak (Figure 2), when the upper-level VHF density maximum was missing from the convective line in general (Figure 3a). However, there was additional evidence for a possible link between graupel at 5–6 km and the development of significant VHF activity in this region, as the maxima in graupel and VHF density were nearly collocated in time and space.

[44] UV10 and UV20 (Figures 7c and 7d) peaked within a few minutes of total flash rate and large hail (Figures 6d and 6e), and the kinematic values were a factor of 2–3 greater than the early hail cells (Figure 7a). UV10 magnitudes were of the same order as the 29 June 2000 +CG-dominated supercell studied by *Tessendorf et al.* [2005], indicating that this was a very intense storm. Again, most of the mixed-phase region was filled by UV10 and UV20. However, updrafts were much weaker after 0035.

[45] Figure 10 shows the evolution of charge in this cell complex. Prior to 0040, a deep layer of positive charge existed throughout the hail-producing southwestern portion (Figure 5c), up to ~10 km MSL (−40°C) with negative charge above. This resembled an inverted dipole [*Rust and MacGorman*, 2002; *Rust et al.*, 2005], and this portion of the storm produced the small number of observed +CGs (Figure 6f). Northeast of this area, in weaker convection, the inverted structure remained but both charge polarities were confined to lower altitudes. In the extreme northeast, by 0045 negative charge existed as low as 5 km MSL (−4°C), with positive charge near 4 km (1°C). This portion of the storm produced most of the −CGs observed after 0040 (Figure 6f).

[46] Figure 11 shows the microphysical and kinematic structure of these cells at 0025, along with an inverted IC that occurred near 0024 in the hail-producing convection. This portion of the storm was very intense, with 10 dBZ reflectivity contours as high as 18 km MSL, and featured many inverted IC flashes like this one. The flash occurred in regions of graupel and hail, near the main updraft of this cell, and revealed the deep layer of positive charge, with negative charge above it extending to 15 km MSL (−55°C; note the blue dots corresponding to negative charge near y = −75 km in Figure 11c and near x = −35 km in Figure 11d).

4.2.4. Severe Wind Cells

[47] Many of the +CGs around 2230 (Figure 2) were produced by a set of cells in the northern end of the convective line, within the bow echo. These cells averaged about 43 km from the LMA network center. The 29 m s^{-1} severe wind report originated from the northern convection at 2217 (Figure 5e). Note, however, that this report may not have been the only instance of severe winds in this MCS, just the only reported instance. Indeed, dual-Doppler analysis showed maximum near-surface horizontal wind speeds to be ~30 m s^{-1} for the period 2200–2225 (not shown). Therefore severe winds probably existed throughout much of the analysis period.

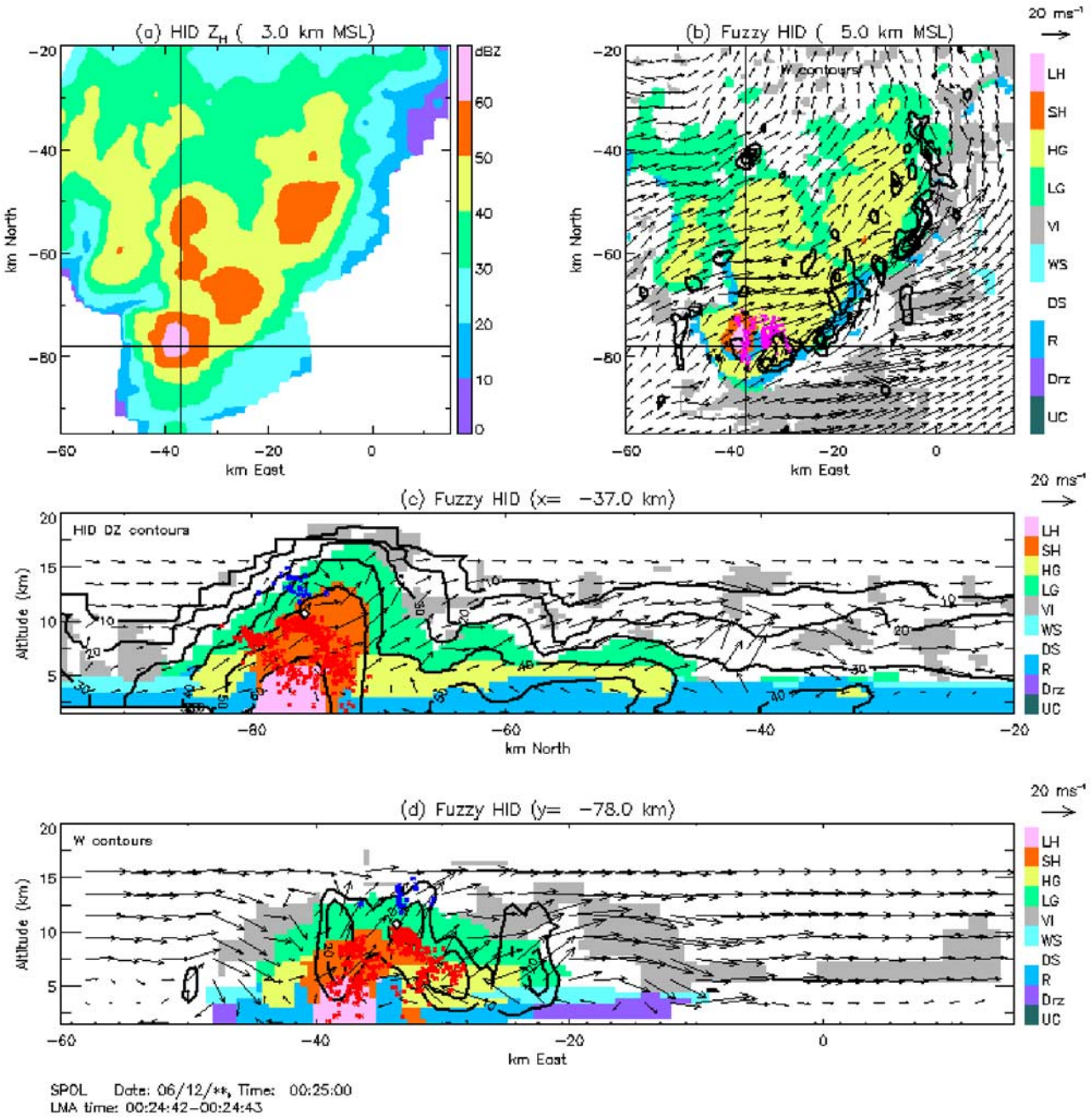

Figure 11. Same as Figure 9 but for the late hail cells at 0024 UTC, with the following differences: (b) One flash at 0024 UTC is shown; (c) and (d) flash initiation point indicated by white diamond.

[48] Figures 6g–6i show the microphysical and electrical evolution of this cell complex during 2150–2240. Once again, graupel was maximized near 5.5 km (Figure 6g). Note that in the last ~20 min of the analysis period, the cells began overrunning S-Pol, making it difficult to capture all of the upper levels on radar. Flash rate followed an increasing trend marked by short-term fluctuations prior to the wind report (Figure 6h), though again it was likely that severe wind speeds were present throughout much of this period. The vertical distribution of VHF source density showed limited evolution, with a maximum near 9 km MSL that broadened downward by 1–2 km after 2210, and weakened after 2220 as graupel volumes decreased (Figures 6g and 6h). Positive CGs occurred throughout the analysis period and were more frequent than −CGs (Figure 6i).

[49] Kinematic statistics were difficult to obtain for these cells, as before 2200 the strongest cores were within the range gap of KGLD Doppler velocities. Later in the time period, not all portions of the complex were scanned or topped by S-Pol. Because of these issues, the UV10 and UV20 statistics (Figures 7e and 7f) likely were underestimates. However, radar coverage was good during 2200–2220, so these values were useful. UV10 and

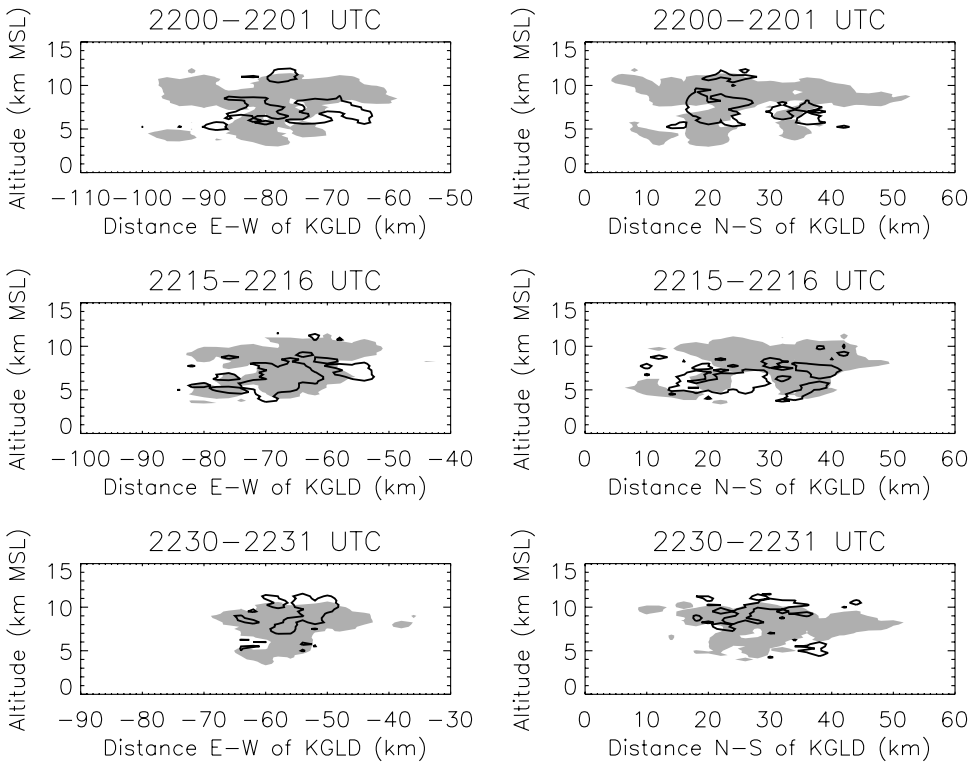

Figure 12. Same as Figure 8 but for the severe wind cells, and contour levels are ±40 km^{-2}.

UV20 were intermediate relative to corresponding values in the other hail cells, and again filled the mixed-phase region. UV10 values were similar to the 29 June 2000 supercell [*Tessendorf et al.*, 2005].

[50] Figure 12 shows the charge evolution, which was extremely complex and resistant to simple categorization. The charge structure also was different than other portions of the convective line at this time (Figure 8). The most persistent feature was a layer of mid-to-upper- level positive charge, which was near 8 km MSL (−23°C) on the northern end of the complex. This northern portion produced most of the +CGs (Figure 6i). The rest of the complex showed substantial heterogeneity, with some normal polarity tripolar and even quadripolar structures around 2200, and more complex structures later in time.

[51] Figure 13 shows the kinematic and microphysical structure of this complex near 2206, along with the electrical structure revealed by a +CG in the north. The +CG occurred outside the main updraft, and part of it propagated to the north, outside the region of graupel and hail where it initiated (Figure 13c). The positive charge layer tapped by this flash ranged within 7–10 km MSL (−16° to −40°C). There was lower negative charge, as well as another negative charge region above the positive charge (e.g., near −80 km E and 12 km MSL in Figure 13d). This resembled an inverted tripole [e.g., *Wiens et al.*, 2005].

[52] There was an interesting cyclonic mesoscale circulation feature at 3 km MSL in the northern portion of this complex, near the +CG (Figure 13b). The strongest winds (∼30 m s^{-1}), from the west-northwest, were located on the southern end of this circulation. This was a cyclonic bookend vortex [*Weisman*, 1993] that existed at 2200, and persisted until at least 2240. Bookend vortices are known to be responsible for the development of severe winds in bow echoes, with the strongest winds commonly observed on the south end of cyclonic vortices [*Weisman*, 1993; *Weisman and Trapp*, 2003; *Trapp and Weisman*, 2003; *Wakimoto et al.*, 2006a, 2006b]. This was true in the present MCS as well. The mesoscale circulation and strong westerly winds were confined mostly below 5 km MSL, which was shallower than some of the strongest modeled or observed bow echoes [e.g., *Weisman and Trapp*, 2003; *Wakimoto et al.*, 2006a, 2006b], and consistent with this bow echo being relatively weak in terms of maximum near-surface wind speeds [e.g., *Weisman*, 2001]. This may have been related to the weak environmental support for bow echoes seen in the sounding from this day (section 2).

4.3. Stratiform Observations

4.3.1. Overview

[53] Analyzing the evolution of the stratiform region of this MCS was difficult, as stratiform flashes were infrequent (Figure 3) and LMA spatial resolution varied significantly as the MCS moved through the network. Nonetheless, there were some interesting findings. Flash rates were examined by type (convective, mixed, stratiform), considering only flashes with VHF source totals greater than 500, and are shown in Figure 14. These large flashes were the easiest and most accurate to classify, both in terms of type and charge. There was a two order of magnitude difference between convective and stratiform flash rates, with large stratiform flashes never averaging more than 1 min^{-1} over a 10-min period. This limited the ability to infer trends within these

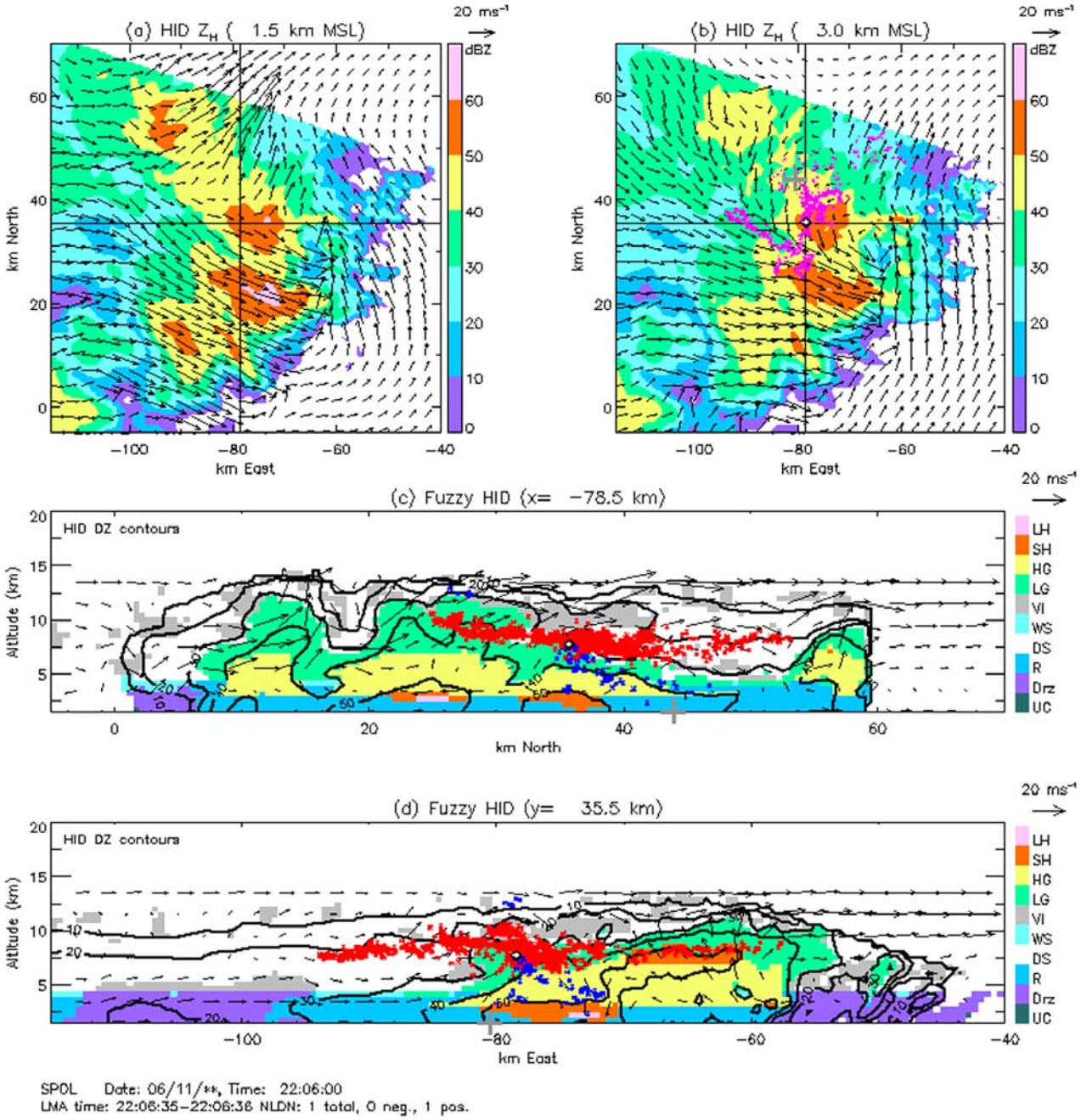

Figure 13. Same as Figure 9 but for the severe wind cells at 2206 UTC, with the following differences: (b) reflectivity and ground-relative dual-Doppler winds, along with one +CG flash at 2206 UTC (+CG strike location is shown as a gray plus sign); (c) and (d) flash initiation point indicated by white diamond, and +CG strike location indicated by the gray plus sign. Also, in Figure 13d reflectivity line contours are shown instead of updraft strength.

flash rates in relation to stratiform reflectivity evolution. However, stratiform flashes were more common after 2300. This roughly coincided with the more vertically intense reflectivity structure after 2300 in the stratiform region. In particular, stratiform flash rates reached their maximum of 1 min^{-1} while 20+ dBZ echoes exceeded 3000 km^3 within the mixed-phase region (Figure 3d). Mixed flash rates fell between the stratiform and convective flash rates, while convective flash rates followed the basic trends established in Figure 2. Note that the peaks in mixed and stratiform flash rates during 2330–0000 may have been partially influenced by the improved LMA resolution in the stratiform region around this time.

4.3.2. Stratiform Charge Structure

[54] *Lang et al.* [2004a] found stratiform +CG VHF sources to average near 6 km (−10°C), a trend confirmed in the present study when considering all types of stratiform flashes (including – CGs and ICs). Figure 15a shows VHF

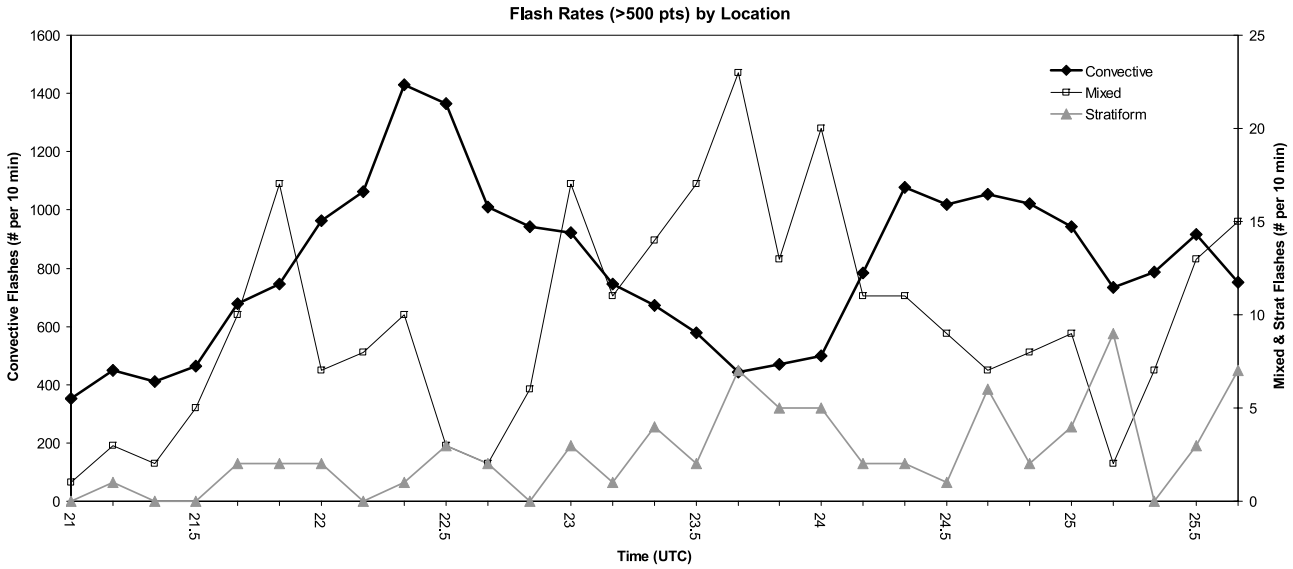

Figure 14. Time series of 10-min convective, mixed, and stratiform flash rates, for flashes containing greater than 500 points (required LMA stations ≥ 6, and $\chi^2 \leq 2.0$ for VHF source locations).

source density associated with positive and negative charge for the stratiform portions of stratiform flashes which occurred in the southern portion of the MCS (defined as −10 to 60 km N of KGLD) during 2340–2350. (Convective components of these flashes were manually edited out.) At this time this portion of the stratiform region was directly over the LMA network, and thus spatial resolution was close to optimum. The positive sources clustered in the

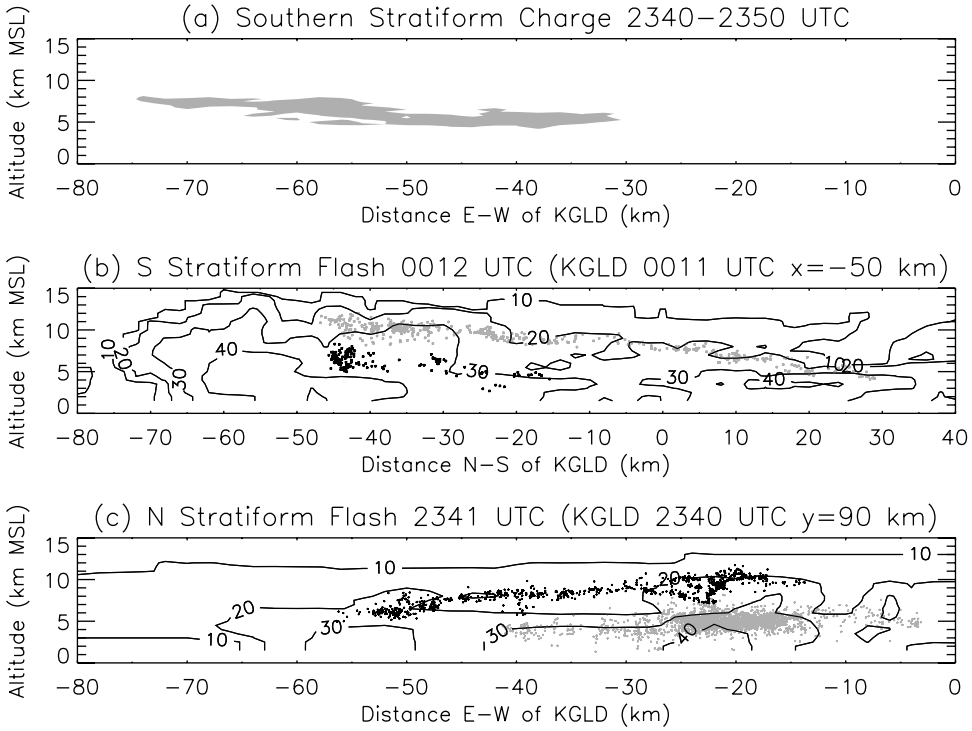

Figure 15. (a) Vertical projection of VHF source density associated with positive (filled gray) and negative (black) charge in the southern portion of the stratiform region, for 2340–2350 UTC. MCS convective line is toward the east, and the N-S slab used for this projection is approximately 70 km thick (−10 to 60 km N of KGLD). Contour levels are ±20 km^{-2}. (b) Vertical cross-section of KGLD reflectivity (line contours in dBZ) at 0011 UTC, and VHF sources associated with a flash in the southern portion of the MCS near 0012 UTC separated by charge similar to Figure 9 (gray, positive, black, negative). E-W slab used for this projection is approximately 30 km thick. (c) Same as Figure 15b but for KGLD at 2340 UTC and a flash in the northern portion of the MCS at 2341 UTC. N-S slab used for this projection is approximately 30 km thick (60 to 90 km N of KGLD). Note the difference in vertical planes between Figures 15b and 15c.

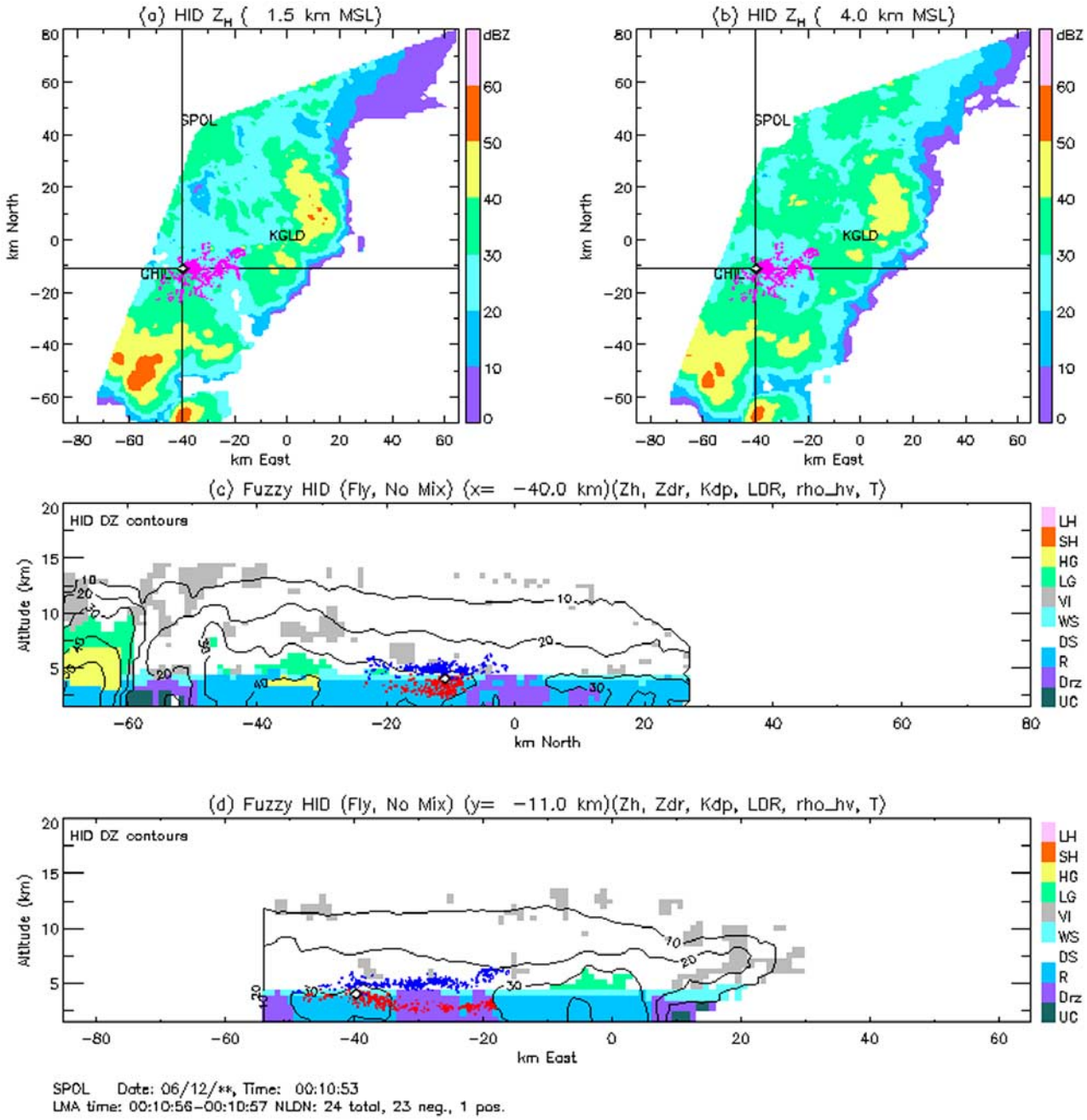

Figure 16. (a) Horizontal cross-section of S-Pol reflectivity for the MCS at 0011 UTC. Lines correspond to vertical cross-sections in Figures 16c and 16d. Also shown are VHF sources for one stratiform-initiated IC flash at 0010 UTC, with its origin (white diamond). (b) Same as Figure 16a but at a higher altitude. (c) Vertical cross-section of HID with the same flash now color coded by charge as in previous plots. (d) Same as Figure 16c but for a different cross-section.

range 5.5–7 km (−7°C to −16°C), with an upward tilt toward the western edge of the stratiform region. This was consistent with the inference of positive charge near 6 km. This charge layer remained active in producing lightning, and its altitude remained approximately constant, with some horizontal heterogeneity, throughout the 5-h observation period.

[55] The lower lightning pathway in the stratiform region was the most common, especially late in this MCS's lifetime. However, there were occasional flashes along a downward-sloping upper pathway, which due to their rarity are difficult to show in the averaged manner of *Carey et al.* [2005]. Some examples of these flashes are shown in Figures 15b and 15c. The first (Figure 15b) was a convective IC with a significant stratiform component, which occurred near 0012 in a decaying cell that had upper positive charge. (Most convection around this time lacked upper positive charge.) This IC was misclassified as a +CG by the NLDN, as the "ground strike" supposedly occurred during rapid upward development of the discharge. The

positive charge component of the flash followed the results of *Carey et al.* [2005], with termination near the bright band in the stratiform region. The flash also followed the downward sloping of the 20-dBZ contour. In addition, the negative portion of the flash sloped downward outside of convection. Though still rare (0–2 per 10-min period), stratiform flashes along a downward-sloping pathway were more common in the early lifetime of the MCS (2100–0000), when upper positive charge appeared in most cells.

[56] The second example was an inverted IC flash that occurred at 2341 in the northern portion of the MCS (defined as 60 to 90 km N of KGLD; Figure 15c). This portion of the storm developed an inverted polarity structure earlier than the southern portion containing the late hail cells, and the upper negative charge sloped downward similar to the upper positive charge in Figure 15b. Recall that around this time the southern portion of the MCS featured stratiform positive charge near 6 km MSL (Figure 15a); this was not as apparent in the northern part of the MCS, where this flash occurred.

4.3.3. Stratiform-Initiated Flashes

[57] Over the entire observation period, 137 flashes (convective, mixed, or stratiform) with 500+ sources were identified as initiating within the stratiform region itself (compared to 22,776 large flashes initiating within the convective line, and 996 within transition areas). A manual analysis of the stratiform-initiated flashes found that at most 25 initiated independently, without any other lightning nearby in time and space. Of the remainder, 10 were misclassified by this study's algorithm due to noise or poor spatial resolution, 16 were due to sparking caused by collisional charging of aircraft in ice clouds [*Thomas et al.*, 2004], and 2 occurred in the forward anvil of the convective line, which also could be classified as stratiform by the algorithm. All other remaining flashes were components of very large complexes of multiple flashes initiating in or near the convective line. The typical pattern was a large convective-initiated flash propagating into the stratiform region, a small gap in time (~50–100 ms), and then the occurrence of a stratiform-initiated flash, beginning near the termination point of the original flash. Because of present uncertainties in the physics of stratiform flashes, it was difficult to say whether this was one large misclassified convective-initiated flash, or multiple flashes. This phenomenon may have been similar to the "associated" lightning flashes studied by *Mazur* [1982] and *Vonnegut et al.* [1985]. These flashes were not considered in the analysis of stratiform-initiated flashes, because they appeared to be related to an initial discharge from the convective line.

[58] Of the 25 independent stratiform-initiated flashes, two occurred during 2320–2330 and the rest all occurred after 0000. One of these flashes is shown in Figure 16. It initiated within the radar bright band (4 km), in wet snow. The stratiform flash subsequently tapped two layers of charge, including negative charge above the melting level and positive charge below (Figures 16c–16d). To the extent that spatial resolution allowed useful analysis, nearly all other stratiform- initiated flashes also occurred near the bright band, initiating between these two charge layers (always negative over positive). These charge layers generally were situated below the main lower positive charge layer that existed around 5.5–7 km MSL (Figure 15a), although multiple flashes tapping these charge layers rarely occurred in the same location (recall that stratiform lightning was infrequent in this storm), and there was some horizontal heterogeneity in flash altitudes in different portions of the stratiform region (e.g., Figure 15a).

5. Discussion and Conclusions

5.1. Convective Evolution

[59] Approximately 99% of VHF lightning sources in the 11–12 June 2000 MCS occurred within 10 km of the convective line. Time-height evolution of VHF sources, as well as an examination of individual convective elements, indicated evolution during the first 3 h within much of the convective line from a normal dipolar charge structure, with upper positive charge near 9 km (−30°C) over mid-level negative charge near 7 km (−16°C), to a normal-polarity tripole with lower positive charge near 4 km (1°C). This tripolar structure, a result of the intensification of the convective line, was broadly consistent with that of the symmetric MCS observed by *Carey et al.* [2005], and was associated with the production of −CG flashes that tapped the lower two charge layers [*Mansell et al.*, 2002].

[60] During the final 2 h, the charge structure resembled an inverted dipole, with negative charge overlaying positive charge. The relative altitudes of these charge layers depended on the intensity of the convection in question. In the most intense cells, such as the southern portion of the late hail cells, the positive charge layer extended up to 10 km (−40°C), with negative charge up to 15 km (−55°C). Cells with these deep positive charge layers sometimes produced +CG lightning. In weaker or decaying cells, such as the northern portion of the late hail cells, the positive charge was as low as 0°C, with negative charge near 5 km (−4°C). These cells sometimes produced −CGs.

[61] A +CG-dominated cell complex was associated with a cyclonic bookend vortex on the northern end of the bow echo. While other portions of the convective line at the same time featured a normal tripole, the bow echo cell complex had an inverted tripolar structure in its northern portion, with mid-level positive charge near 8 km (−23°C). In the southern portion the charge structure was extremely complex and defied simple categorization. The fact that these charge structures were associated solely with the bow echo suggests that future work should examine if cells associated with bow echoes commonly feature atypical charge structures and lightning. In addition, because of the differences between the bow echo cells and the rest of the convective line at this time (e.g., the early hail cells), this study establishes that asymmetries in charge structure can occur within the convective line of asymmetric MCSs, as hypothesized.

[62] The various inverted electrical structures observed in this MCS were very similar to those in other STEPS storms analyzed by *Rust and MacGorman* [2002], *Lang et al.* [2004b], *Rust et al.* [2005] and *Wiens et al.* [2005], with positive charge layers of varying depths located at mid-levels within the storm (e.g., −10 to −20°C). Additionally, these inverted structures produced predominantly +CG lightning (except during decay), similar to previous studies. These results suggest that convective +CGs in other MCSs

[e.g., *Knupp et al.*, 1998] also may be produced by inverted charge structures.

[63] The results of this study were consistent with those of *Wiens et al.* [2005], as the inverted charge structures were associated with large volumes of strong updrafts. As *Lang and Rutledge* [2002] and *Wiens et al.* [2005] argued, stronger and broader updrafts should produce higher liquid water contents, which would boost riming accretion rates and enhance the probability of the riming particle gaining positive charge at colder temperatures [e.g., *Saunders and Peck*, 1998]. Environmental data were not examined for possible clues as to why this storm-wide change occurred, though the inverted structures occurred first in the northern portions of the MCS (Figure 15c).

[64] In the severe portions of the MCS, large hail and strong winds usually were associated with enhanced total lightning flash rate, increased VHF source density, and upward pulses in VHF source altitudes. Additionally, these lightning phenomena often occurred several minutes prior to the occurrence of large hail. This expected result supports the conclusions of *Williams et al.* [1999] and *Hamlin et al.* [2001], and suggests that relationships between lightning and severe weather in the convective line of MCSs are similar to those seen in isolated convection. The observed changes in the gross vertical distribution of VHF sources (e.g., Figures 3 and 6), coupled with the development of graupel at low levels, may be important. Consistent with non-inductive charging theory, both observations [e.g., *Wiens et al.*, 2005] and model simulations [e.g., *Kuhlman et al.*, 2006] support the inference that total lightning flash rate should reveal the development of graupel, as observed. The present study adds to previous work by suggesting that the vertical distribution of VHF lightning could be used as a proxy for locating graupel. Note that this study and *Tessendorf et al.* [2005] showed that the development of significant amounts of graupel often was associated with the occurrence of large hail. This raises the possibility that changes in the vertical distribution of VHF sources could consistently precede the occurrence of large hail, as observed in this study. This may add another potential severe weather "nowcasting" role for VHF lightning mapping data.

5.2. Stratiform Evolution

[65] In contrast with previous studies of asymmetric and bow-echo MCSs, the stratiform charge structure in this MCS was similar to symmetric MCSs [*Schuur and Rutledge*, 2000a; *Carey et al.*, 2005], and most similar to the Type A charge structure archetype of *Marshall and Rust* [1993]. Positive charge existed near −10°C, and was the primary conduit for stratiform lightning initiated in convection. There was evidence that this positive charge layer was elevated in height far from the convective line, a finding not represented in current conceptual models of stratiform electrification and charge structure [*Stolzenburg et al.*, 1998]. The elevation of this layer may have been caused by the horizontal transport and weak lifting of positively charged cloud particles within the base of the ascending front-to-rear flow that exists in many MCSs [*Houze et al.*, 1990].

[66] A secondary conduit containing positive charge existed along a downward-sloping upper pathway that started near −30°C and terminated near the bright band. Negative charge existed near 0°C, with another positive charge layer below this at temperatures above freezing. Because of a relative lack of stratiform flashes, and variability in LMA spatial resolution because of storm motion, there was little evidence that this basic charge structure evolved in time. It appeared to not evolve, except that the sloping upper positive charge was replaced by negative charge once inverted-polarity charge structures occurred in the convective line.

[67] This study's results support the basic inferences of *Carey et al.* [2005] that the sloping upper charge layer (positive or negative) in MCSs is caused by advection of charged ice particles, especially snow, from the convective line. However, as *Carey et al.* [2005] noted, this does not rule out an in situ charging mechanism also being active in this layer as it descends.

[68] The increase in vertical reflectivity intensity after 2300 in the STEPS MCS, along with the approximately stationary positive charge layer at −10°C, was suggestive of an in situ mechanism being active in this layer, following the arguments of *Carey et al.* [2005] and other studies. In addition, the polarity switch in charge layers above and below the melting level was suggestive of an in situ charging mechanism based on melting in this region [*Shepherd et al.*, 1996]. Whatever the nature of this speculated melting electrification mechanism (e.g., [see *Shepherd et al.*, 1996] for different possibilities), it was evidently the one most capable of generating strong enough electric fields to initiate lightning within the stratiform region itself, as opposed to merely providing a conduit for lightning initiated in the convective line. Moreover, the observation that nearly all stratiform-initiated flashes started near the bright band was consistent with the well-known enhanced lightning hazard to aircraft flying near this altitude in MCSs [e.g., *Davis et al.*, 2004].

[69] **Acknowledgments.** We thank Kyle Wiens, Sarah Tessendorf, and Larry Carey for their valuable discussions and assistance with this research. LMA data were provided by Paul Krehbiel, who also provided substantial assistance with their interpretation and analysis, as well as provided insightful comments and suggestions on the manuscript. Dave Rust and Don MacGorman of NOAA/NSSL provided the balloon sounding data. NLDN data were provided by Vaisala. S-Pol and KGLD data were provided by NCAR. This research was funded by National Science Foundation grant ATM-0309303 from the Physical Meteorology program. The S-Pol radar is supported by the National Science Foundation.

References

Carey, L., and S. Rutledge (1998), Electrical and multiparameter radar observations of a severe hailstorm, *J. Geophys. Res.*, *103*(D12), 13,979–14,000.

Carey, L. D., S. A. Rutledge, and W. A. Petersen (2003), The relationship between severe storm reports and cloud-to-ground lightning in the contiguous United States from 1989 to 1998, *Mon. Weather Rev.*, *131*, 1211–1228.

Carey, L. D., M. J. Murphy, T. L. McCormick, and N. W. S. Demetriades (2005), Lightning location relative to storm structure in a leading-line, trailing-stratiform mesoscale convective system, *J. Geophys. Res.*, *110*, D03105, doi:10.1029/2003JD004371.

Coleman, L. M., T. C. Marshall, M. Stolzenburg, T. Hamlin, P. R. Krehbiel, W. Rison, and R. J. Thomas (2003), Effects of charge and electrostatic potential on lightning propagation, *J. Geophys. Res.*, *108*(D9), 4298, doi:10.1029/2002JD002718.

Cummins, K. L., M. J. Murphy, E. A. Bardo, W. L. Hiscox, R. B. Pyle, and A. E. Pifer (1998), A combined TOA/MDF technology upgrade of the U.S National Lightning Detection Network, *J. Geophys. Res.*, *103*(D8), 9035–9044.

Davis, C., et al. (2004), The bow echo and MCV experiment: Observations and opportunities, *Bull Am. Meteorol. Soc.*, *85*, 1075–1093.

Hamlin, T., J. D. Harlin, P. R. Krehbiel, W. Rison, and R. J. Thomas (2001), Lightning as a detector of convective surges in thunderstorms, *Eos Trans. Am. Geophys. Union*, *82*(Suppl.), Abstract AE12A-86.

Hill, R. D. (1988), Interpretation of bipole patterns in a mesoscale storm, *Geophys. Res. Lett.*, *15*(7), 643–644.

Houze, R. A., Jr., B. F. Smull, and P. Dodge (1990), Mesoscale organization of springtime rainstorms in Oklahoma, *Mon. Weather Rev.*, *118*, 613–654.

Kasemir, H. W. (1960), A contribution to the electrostatic theory of lightning discharge, *J. Geophys. Res.*, *65*(7), 1873–1878.

Knupp, K. R., B. Geerts, and S. J. Goodman (1998), Analysis of a small, vigorous, mesoscale convective system in a low-shear environment. Part I: Formation, radar echo structure, and lightning behavior, *Mon. Weather Rev.*, *126*, 1812–1836.

Kuhlman, K. M., C. L. Ziegler, E. R. Mansell, D. R. MacGorman, and J. M. Straka (2006), Numerically simulated electrification and lightning of the 29 June 2000 STEPS supercell storm, *Mon. Weather Rev.*, *134*, 2734–2757.

Lang, T. J., and S. A. Rutledge (2002), Relationships between convective storm kinematics, precipitation, and lightning, *Mon. Weather Rev.*, *130*, 2492–2506.

Lang, T. J., S. A. Rutledge, J. E. Dye, M. Venticinque, P. Laroche, and E. Defer (2000), Anomalously low negative cloud-to-ground lightning flash rates in intense convective storms observed during STERAO-A, *Mon. Weather Rev.*, *128*, 160–173.

Lang, T. J., S. A. Rutledge, and K. C. Wiens (2004a), Origins of positive cloud-to-ground lightning flashes in the stratiform region of a mesoscale convective system, *Geophys. Res. Lett.*, *31*, L10105, doi:10.1029/2004GL019823.

Lang, T. J., et al. (2004b), The Severe Thunderstorm Electrification and Precipitation Study (STEPS), *Bull. Am. Meteorol. Soc.*, *85*, 1107–1125.

Lyons, W. A., T. E. Nelson, E. R. Williams, S. A. Cummer, and M. A. Stanley (2003), Characteristics of sprite-producing positive cloud-to-ground lightning during the 19 July 2000 STEPS mesoscale convective systems, *Mon. Weather Rev.*, *131*, 2417–2427.

MacGorman, D. R., D. W. Burgess, V. Mazur, W. D. Rust, W. L. Taylor, and B. C. Johnson (1989), Lightning rates relative to tornadic storm evolution on 22 May 1981, *J. Atmos. Sci.*, *46*, 221–251.

Mansell, E. R., D. R. MacGorman, C. L. Ziegler, and J. M. Straka (2002), Simulated three-dimensional branched lightning in a numerical thunderstorm model, *J. Geophys. Res.*, *107*(D9), 4075, doi:10.1029/2000JD000244.

Marshall, T. C., and W. D. Rust (1993), Two types of vertical electrical structures in stratiform precipitation regions of mesoscale convective systems, *Bull. Am. Meteorol. Soc.*, *74*, 2159–2170.

Mazur, V. (1982), Associated lightning discharges, *Geophys. Res. Lett.*, *9*(11), 1227–1230.

Mazur, V., and L. H. Ruhnke (1993), Common physical processes in natural and artificially triggered lightning, *J. Geophys. Res.*, *98*(D7), 12,913–12,930.

Nielsen, K. E., R. A. Maddox, and S. V. Vasiloff (1994), The evolution of cloud-to-ground lightning within a portion of the 10–11 June 1985 squall line, *Mon. Weather Rev.*, *122*, 1809–1817.

Orville, R. E., R. W. Henderson, and L. F. Bosart (1988), Bipole patterns revealed by lightning locations in mesoscale storm systems, *Geophys. Res. Lett.*, *15*(2), 129–132.

Petersen, W. A., S. A. Rutledge, and R. E. Orville (1996), Cloud-to-ground lightning observations from TOGA COARE: Selected results and lightning location algorithms, *Mon. Weather Rev.*, *124*, 602–620.

Price, C. G., and B. P. Murphy (2002), Lightning activity during the 1999 Superior derecho, *Geophys. Res. Lett.*, *29*(23), 2142, doi:10.1029/2002GL015488.

Rison, W., R. J. Thomas, P. R. Krehbiel, T. Hamlin, and J. Harlin (1999), A GPS-based three-dimensional lightning mapping system: Initial observations in central New Mexico, *Geophys. Res. Lett.*, *26*(23), 3573–3576.

Rust, W. D., and D. R. MacGorman (2002), Possibly inverted-polarity electrical structures in thunderstorms during STEPS, *Geophys. Res. Lett.*, *29*(12), 1571, doi:10.1029/2001GL014303.

Rust, W. D., D. R. MacGorman, and R. T. Arnold (1981a), Positive cloud-to-ground lightning flashes in severe storms, *Geophys. Res. Lett.*, *8*(7), 791–794.

Rust, W. D., D. R. MacGorman, and R. T. Arnold (1981b), Research on the electrical properties of severe thunderstorms in the Great Plains, *Bull. Am. Meteorol.*, *62*, 1286–1293.

Rust, W. D., D. R. MacGorman, E. C. Buning, S. A. Weiss, P. R. Krehbiel, R. J. Thomas, W. Rison, and J. Harlin (2005), Inverted-polarity electrical structures in thunderstorms in the Severe Thunderstorm Electrification Study (STEPS), *Atmos. Res.*, doi:10.1016/j.atmosres.2004.11.029.

Rutledge, S. A., and D. R. MacGorman (1988), Cloud-to-ground lightning activity in the 10–11 June 1985 mesoscale convective system observed during the Oklahoma-Kansas PRE-STORM project, *Mon. Weather Rev.*, *116*, 1393–1408.

Rutledge, S. A., and W. A. Petersen (1994), Vertical radar reflectivity structure and cloud-to-ground lightning in the stratiform region of MCSs: Further evidence for in situ charging in the stratiform region, *Mon. Weather Rev.*, *122*, 1760–1776.

Rutledge, S. A., C. Lu, and D. R. MacGorman (1990), Positive cloud-to-ground lightning in mesoscale convective systems, *J. Atmos. Sci.*, *47*, 2085–2100.

Rutledge, S. A., E. R. Williams, and W. A. Petersen (1993), Lightning and electrical structure of mesoscale convective systems, *Atmos. Res.*, *29*, 27–53.

Saunders, C. P. R., and S. L. Peck (1998), Laboratory studies of the influence of the rime accretion rate on charge transfer during graupel/crystal collisions, *J. Geophys. Res.*, *103*(D12), 13,949–13,956.

Schuur, T. J., and S. A. Rutledge (2000a), Electrification of stratiform regions in mesoscale convective systems. Part I: An observational comparison of symmetric and asymmetric MCSs, *J. Atmos. Sci.*, *57*, 1961–1982.

Schuur, T. J., and S. A. Rutledge (2000b), Electrification of stratiform regions in mesoscale convective systems. Part II: Two-dimensional numerical model simulations of a symmetric MCS, *J. Atmos. Sci.*, *57*, 1983–2006.

Shepherd, T. R., W. D. Rust, and T. C. Marshall (1996), Electric fields and charges near 0°C in stratiform clouds, *Mon. Weather Rev.*, *124*, 919–938.

Steiner, M., R. A. Houze Jr., and S. E. Yuter (1995), Climatological characterization of three-dimensional storm structure from operational radar and rain gauge data, *J. Appl. Meteorol.*, *34*, 1978–2007.

Stolzenburg, M. (1990), Characteristic of the bipolar pattern of lightning locations observed in 1988 thunderstorms, *Bull. Am. Meteorol. Soc.*, *71*, 1331–1338.

Stolzenburg, M. (1994), Observations of high ground flash densities of positive lightning in summertime thunderstorms, *Mon. Weather Rev.*, *122*, 1740–1750.

Stolzenburg, M., W. D. Rust, B. F. Smull, and T. C. Marshall (1998), Electrical structure in thunderstorm convective regions. 1. Mesoscale convective systems, *J. Geophys. Res.*, *103*(D12), 14,059–14,078.

Stolzenburg, M., T. C. Marshall, and W. D. Rust (2001), Serial soundings of electric field through the mesoscale convective system, *J. Geophys. Res.*, *106*(D12), 12,371–12,380.

Tessendorf, S. A., L. J. Miller, K. C. Wiens, and S. A. Rutledge (2005), The 29 June 2000 supercell observed during STEPS. Part I: Kinematics and microphysics, *J. Atmos. Sci.*, *62*, 4127–4150.

Thomas, R. J., T. Hamlin, J. Harlin, P. Krehbiel, W. Rison, and M. Stanley (2001), Thunderstorm charge structure and the spatial distribution of radiation sources located by the LMA. Abstract AE12A-0081, *Fall Ann. Mtg. Am. Geophys. Union EOS Trans. AGU*, *82*(47).

Thomas, R., P. Krehbiel, W. Rison, J. Harlin, T. Hamlin, and N. Campbell (2003), The LMA flash algorithm, in *11th Int. Conf. on Atmos. Electr.*, Int. Commission on Atmospheric, Versailles, France, pp. 655–656.

Thomas, R. J., P. R. Krehbiel, W. Rison, S. J. Hunyady, W. P. Winn, T. Hamlin, and J. Harlin (2004), Accuracy of the lightning mapping array, *J. Geophys. Res.*, *109*, D14207, doi:10.1029/2004JD004549.

Trapp, R. J., and M. L. Weisman (2003), Low-level mesovortices within squall lines and bow echoes. Part II: Their genesis and implications, *Mon. Weather Rev.*, *131*, 2804–2823.

Vonnegut, B., O. H. Vaughan Jr., M. Brook, and P. Krehbiel (1985), Mesoscale observations of lightning from space shuttle, *Bull. Am. Meteorol. Soc.*, *66*, 20–29.

Wakimoto, R. M., H. V. Murphey, A. Nester, D. P. Jorgensen, and N. T. Atkins (2006a), High winds generated by bow echoes. Part I: Overview of the Omaha bow echo 5 July 2003 storm during BAMEX, *Mon. Weather Rev.*, *134*, 2793–2812.

Wakimoto, R. M., H. V. Murphey, C. A. Davis, and N. T. Atkins (2006b), High winds generated by bow echoes. Part II: The relationship between the mesovortices and damaging straight-line winds, *Mon. Weather Rev.*, *134*, 2813–2829.

Weisman, M. L. (1993), The genesis of severe, long-lived bow echoes, *J. Atmos. Sci.*, *50*, 645–670.

Weisman, M. L. (2001), Bow echoes: A tribute to T. T. Fujita, *Bull. Am. Meteorol. Soc.*, *82*, 97–116.

Weisman, M. L., and J. B. Klemp (1986), *Characteristics of Isolated Convective Storms. Mesoscale Meteorology and Forecasting*, edited by Peter S. Ray, *Amer. Meteor. Soc.*, pp. 331–358.

Weisman, M. L., and R. J. Trapp (2003), Low-level mesovortices within squall lines and bow echoes. Part I: Overview and dependence on environmental shear, *Mon. Weather Rev.*, *131*, 2779–2803.

Wiens, K. C., S. A. Rutledge, and S. A. Tessendorf (2005), The 29 June 2000 supercell observed during STEPS. Part II: Lightning and charge structure, *J. Atmos. Sci.*, *62*, 4151–4177.

Williams, E. R. (1989), The tripole structure of thunderstorms, *J. Geophys. Res.*, *94*(D11), 13,151–13,167.

Williams, E., B. Boldi, A. Matlin, M. Weber, S. Hodanish, D. Sharp, S. Goodman, R. Raghavan, and D. Buechler (1999), The behavior of total lightning activity in severe Florida thunderstorms, *Atmos. Res.*, *51*, 245–265.

Williams, E. R., V. Mushtak, D. Rosenfeld, S. Goodman, and D. Boccippio (2005), Thermodynamic conditions favorable to superlative thunderstorm updraft, mixed phase microphysics and lightning flash rate, *Atmos. Res.*, *76*, 288–306.

Witt, A., M. D. Eilts, G. J. Stumpf, J. T. Johnson, E. D. Mitchell, and K. W. Thomas (1998a), An enhanced hail detection algorithm for the WSR-88D, *Weather Forecasting*, *13*, 286–303.

Witt, A., M. D. Eilts, G. J. Stumpf, E. D. Mitchell, J. T. Johnson, and K. W. Thomas (1998b), Evaluating the performance of WSR-88D severe storm detection algorithms, *Weather Forecasting*, *13*, 513–518.

Yuter, S. E., and R. A. Houze Jr. (1998), The natural variability of precipitating clouds over the western Pacific warm pool, *Q. J. R. Meteorol. Soc.*, *124*, 53–99.

T. J. Lang and S. A. Rutledge, Department of Atmospheric Science, Colorado State University, 200 West Lake Street, Fort Collins, CO 80523, USA. (tlang@atmos.colostate.edu)